A predicted CRISPR-mediated symbiosis between uncultivated archaea

Sarah P. Esser[1,2,*], Janina Rahlff[2,*,†], Weishu Zhao[3,††], Michael Predl[4,5], Julia Plewka[1,2], Katharina Sures[1,2], Franziska Wimmer[6], Janey Lee[7], Panagiotis S. Adam[2], Julia McGonigle[8], Victoria Turzynski[1,2], Indra Banas[1,2], Katrin Schwank[2,†††], Mart Krupovic[9], Till L. V. Bornemann[1,2], Perla Abigail Figueroa-Gonzalez[1,2], Jessica Jarett[7], Thomas Rattei[4,5], Yuki Amano[10], Ian K. Blaby[7], Jan-Fang Cheng[7], William J. Brazelton[8], Chase L. Beisel[6,11], Tanja Woyke[7], Ying Zhang[3], and Alexander J. Probst[1,2,12,13,#]

[1]Environmental Metagenomics, Research Center One Health of the University Alliance Ruhr, Faculty of Chemistry, University of Duisburg-Essen, 45151 Essen

[2]Group for Aquatic Microbial Ecology, Environmental Microbiology and Biotechnology, University of Duisburg-Essen, 45141 Essen

[3]Department of Cell and Molecular Biology, College of the Environment and Life Sciences, University of Rhode Island, Kingston, RI 02881, USA

[4]Computational Systems Biology, Centre for Microbiology and Environmental Systems Science, University of Vienna, 1030 Vienna, Austria

[5]Doctoral School in Microbiology and Environmental Science, University of Vienna, 1030 Vienna, Austria

[6]Helmholtz Institute for RNA-based Infection Research (HIRI), Helmholtz-Centre for Infection Research (HZI), 97080 Würzburg, Germany

[7]DOE Joint Genome Institute, Lawrence Berkeley National Laboratory, One Cyclotron Rd, Berkeley, CA, 94720, USA

[8]School of Biological Sciences, University of Utah, Salt Lake City, Utah, USA

[9]Institut Pasteur, Université Paris Cité, CNRS UMR6047, Archaeal Virology Unit, 75015 Paris, France

[10]Nuclear Fuel Cycle Engineering Laboratories, Japan Atomic Energy Agency, Tokai, Ibaraki, 319-1194 Japan

[11]Medical faculty, University of Würzburg, 97080 Würzburg Germany

[12]Centre of Water and Environmental Research (ZWU), University of Duisburg-Essen, 45141 Essen, Germany

[13]Centre of Medical Biotechnology (ZMB), University of Duisburg-Essen, 45141 Essen, Germany

[*]authors contributed equally

[†]present address: Centre for Ecology and Evolution in Microbial Model Systems (EEMiS), Department of Biology and Environmental Science, Linnaeus University, Kalmar, Sweden

[††]present address: Shanghai Jiao Tong University, School of Life Sciences and Biotechnology, International Center for Deep Life Investigation (IC-DLI), Shanghai Jiao Tong University, Shanghai, 200240, China

[†††]present address: University of Regensburg, Biochemistry III, 93053 Regensburg, Germany

[#]corresponding author: alexander.probst@uni-due.de

ABSTRACT

CRISPR-Cas systems defend prokaryotic cells from invasive DNA of viruses, plasmids, and other mobile genetic elements. Here we show using metagenomics, metatranscriptomics and single-cell genomics that CRISPR systems of widespread, uncultivated archaea can also target chromosomal DNA of archaeal episymbionts of the DPANN superphylum. Using meta-omics datasets from Crystal Geyser (USA) and Horonobe Underground Research Laboratory (Japan), we find that CRISPR spacers of the hosts *Candidatus* Altiarchaeum crystalense and *Ca.* A. horonobense, respectively, match putative essential genes in their episymbionts' genomes of the genus *Ca.* Huberiarchaeum, and that some of these spacers are expressed *in situ*. Metabolic interaction modeling also reveals complementation between host-episymbiont systems, based on which we propose that episymbionts are either parasitic or mutualistic depending on the genotype of the host. By expanding our analysis to 7,012 archaeal genomes, we suggest that CRISPR-Cas targeting of genomes associated with symbiotic archaea evolved independently in various archaeal lineages.

INTRODUCTION

Clustered regularly interspaced short palindromic repeats associated systems (CRISPR-Cas) facilitate adaptive prokaryotic immunity via cleavage of mobile genetic elements (MGEs), e.g., viruses and plasmids[1]. CRISPR *loci* consist of a series of direct repeat (DR) sequences interspaced by short variable fragments, *i.e.*, spacers, flanked by *cas* genes. Upon exposure to novel MGEs, short DNA fragments from these invaders are incorporated into the CRISPR array as spacers. The spacers are then used as templates to form CRISPR RNAs (crRNAs) that guide effector Cas nucleases to complementary nucleic acid sequences. Spacer sequences can also be used to study infection histories *in silico* based on matches to protospacers, corresponding nucleic acid regions in the MGE[2].

CRISPR systems exhibit remarkable diversity and functional plasticity including roles in non-defensive functions (reviewed by Koonin & Makarova 2022[3]). Six main types of CRISPR-Cas systems have been described, including different subtypes, *e.g.*, type I-A to I-F, depending on

signature genes and their arrangements[4,5]. Target identification in type I and II systems is dependent on the recognition of a short protospacer-adjacent motif (PAM) in the target DNA sequence, which elicits cleavage and clearance of the MGE's protospacer. Rather than relying on a defined PAM for target recognition, other CRISPR systems (*e.g.* type III) generally evaluate the extent of hybridization between the flanking portions of the crRNA (called protospacer-flanking sequence) and the target[6,7]. While CRISPR-Cas systems are widely distributed, they are more common in archaea (in ~85% of genomes) than in bacteria (in ~40% of genomes; reviewed by Makarova et al. 2020)[5].

Branching from the archaeal tree of life, the DPANN superphylum including *i.e.*, Diapherotrites, Parvarchaeota, Aenigmarchaeota, Nanoarchaeota and Nanohaloarchaeota, and several other recently proposed phyla[8,9], comprises a vast collection of microorganisms remarkably small in size and enigmatic due to the scarcity of cultivated representatives[10,11]. Insights into the physiological characteristics of DPANN archaea arise primarily from detailed analyses of co-cultivation with amenable microorganisms[12,13] and/or imaging of environmental samples[14]. These inferences, along with the limited metabolic potential contained in their comparatively small genomes, suggest that most DPANN archaea exist as (epi-)symbionts of other archaea[13,15–18] or even as intracellular symbionts[19]. The independent and autotrophic *Candidatus* Altiarchaeum sp. is host organism to another uncultivated DPANN archaeon, *Candidatus* Huberiarchaeum crystalense[14,20].

Previous evidence suggested that certain DPANN archaea can fuse their cytoplasm with that of their hosts[14,15,21–23] and even exchange enzymes[21]. Cytoplasm fusion could in theory facilitate transfer of metabolites from the host to the symbiont consequently rendering such a symbiosis potentially parasitic. Hence, we investigated the symbiotic nature of the uncultivated DPANN *Ca.* Altiarchaeum and its uncultivated DPANN episymbiont *Ca.* Huberiarchaeum using meta-omics and metabolic modeling in two independent subsurface ecosystems (Fig. 1A). Based on the complex interaction of *Ca.* Altiarchaea and viruses in deep subsurface ecosystems, we examined the encoded CRISPR systems and analyzed the targets of their respective spacer populations in two independent subsurface ecosystems (accessible through Crystal Geyser (CG), Utah, USA and Horonobe Underground Research Laboratory (HURL), Hokkaido, Japan), where we

identified both the host, and the symbiont being associated based on fluorescence *in situ* hybridization (FISH). Our findings demonstrate that a substantial portion of the host spacer population is targeted towards the genomes of the episymbionts having the same PAM sequence as the respectively targeted viruses in the ecosystems. In addition, the host CRISPR systems also target the host chromosome, based on which genome-centric metabolic modeling predicted a mutualistic relationship between host and episymbiont as a function of metabolic complementation. Based on our results, we suggest that CRISPR-Cas systems play an integral role in mediating archaeal host-DPANN interactions.

RESULTS

A CRISPR-Cas system targets archaeal episymbiont genomes

Two subsurface ecosystems separated by 8,255 km (Fig. 1A) and derived from different geological formations[20,24]*, i.e.*, a Wingate Sandstone-hosted aquifer of the Colorado Plateau at ~ 350 m depth (the CG ecosystem)[20,25–27] and a diatomaceous/siliceous mudstone-hosted aquifer of the HURL[24] at ~ 250 m depth, were dominated by two species of *Ca.* Altiarchaea (up to 24.5% and 51.6% of the community, respectively). We show their association with cells of *Ca.* Huberiarchaea, their DPANN episymbiont, using species-specific FISH (Fig. 1A). The *Ca.* Altiarchaea genomes retrieved from CG and HURL were shown to encode a I-B CRISPR system and an abundant CRISPR array, which could not be assigned to a specific *cas* gene casette, as has been reported for other *Ca.* Altiarchaea species[25,28]. Confidence in assigning the CRISPR-Cas system to its correct metagenome-assembled genome (MAG; Altiarchaea genomes n=1; Table S1-S2) derives from the exceedingly high abundance of *Ca.* Altiarchaea genome fragments in the CG samples (Fig. S1). In addition, within 219 single-cell amplified genomes (SAGs; Altiarchaea SAGs n=7; Table S3) from CG, only *Ca.* Altiarchaea bore the corresponding consensus DR sequence (see Extended Data Fig. 1 for additional correlation-based evidence), which were remarkably well-conserved across ecosystems[28] (Fig. 1B).

Analyses of spacers from *Ca.* Altiarchaeum crystalense detected in 66 CG metagenomes over six years of surveillance (1.07 Tbps of sequencing data, Table S1) revealed 297,531 distinct spacer clusters (Fig. 1B), indicative of a complex CRISPR spacer repertoire system for this

organism (Figs. S2 and S3). Within these metagenomes, CRISPR type I-B spacers matched the protospacers of 64 viral DNA sequences corresponding to 14 distinct viral genus clusters (Fig. 1C, Table S6, Extended Data Fig. 2, Fig. S4-S6, details in Supplementary Results). The PAM sequence 5'-TTN-3' was identified on viral targets matched by type I-B spacers (Fig. S7). However, we were unable to experimentally confirm this PAM using an established PAM assay[29] or to assess GFP repression[30] using the 5'-TTN-3' PAM in a cell-free transcription-translation (TXTL) system[29], likely due to the divergent settings (including temperature) of the host environment compared to those used in the established assay[29].

The finding that all virus-matched spacers detected in the exhaustive CG survey derived from the CRISPR I-B system and the ubiquitous nature of this system in *Ca.* Altiarchaea worldwide[28] suggests that the I-B system serves as a primary line of defense against viruses infecting these archaea. A substantial fraction of the spacers matched microbial genomes, including those of *Ca.* A. crystalense, *i.e.*, its own genome (self-targeting, up to 2.9% in sample CG16) and of its episymbiont *Ca.* Huberiarchaeum crystalense (up to 2.8% in sample CG08; Fig. 1C-1D, Fig. 2A-D). The relative proportion of spacers matching the episymbiont was greater than that matching the host genome (Fig. 1C-D), indicative of biased acquisition, negative selection of self-targeting spacers or a positive selection for spacers from the episymbiont genome. The positions of these spacers in the CRISPR I-B array encoded in an altiarchaeal SAG suggest that these spacers prevailed in the system for extended periods (Fig. 2D). While 17% of the protospacers self-targeted through the I-B system showed a significant decrease in metagenomic coverage compared to untargeted scaffold regions (bootstrapped Wilcoxon paired signed rank test, target sites = 196, FDR-corrected p-value < 0.05), 30% of the I-B protospacers in *Ca.* H. crystalense genomes showed a significant drop in coverage, suggesting *in situ* targeting of the episymbiont in CG (bootstrapped Wilcoxon signed rank test, target sites = 73, FDR-corrected p-value < 0.05; Supplementary Results, Extended Data Fig. 3). The coverage of the significantly different targeted regions, compared to the average coverage of the scaffold decreases in *Ca.* A. crystalense and *Ca.* H. crystalense by 10.74% (median) and 36.99% (median), respectively (bootstrapped Wilcoxon signed rank test, n=990, FDR-corrected p-value < 0.05; details in Supplementary Results, Table S5). Supporting this difference, the PAM sequence detected next

to the protospacers in *Ca.* H. crystalense was identical to that of the virus-targeting PAM sequence (Fig. S7). Coverage drops as observed herein could also arise from misassemblies, regions excised in subpopulations, or elevated SNPs resulting in low recruitment of reads.

In contrast to the conserved PAM in the episymbiont and the viruses, the self-targeted protospacer regions were not associated with the 5'-TTN-3' PAM (Fig. S7). As shown for other microbial communities, self-targeting can result in cell suicide (reviewed in Heussler and O'Toole, 2016)[31] or transcriptional regulation[32] of genes influencing the fitness of the microbial population and can thus reduce the strain variation within an ecosystem[33]. However, the lack of the PAM, the essential motif for successful targeting of DNA by CRISPR system type I (reviewed in Bhaya *et al.* 2011)[34] in the population genomes of *Ca.* Altiarchaea, might on the one hand prevent subpopulations of *Ca.* Altiarchaea from cell death by autoimmunity. On the other hand, the correct PAM could still lead to cell death in subpopulations, given that the PAM has not been silenced by mutations. Based on the overall results from metagenomics and metatranscriptomics we suggest that CRISPR-Cas systems may function similarly against viral DNA and chromosomal DNA of episymbionts.

Previous investigations, which were based on either species-specific FISH or electron microscopy, indicate that many DPANN archaea (including *Ca.* A. crystalense and its episymbiont) fuse their cytoplasms[14,15,21–23]. This direct interaction of the host's and the symbiont's cytoplasms, and a potentially predatory nature of the symbiont[14,20], likely underlie the evolution of a direct assault on the episymbiont's genome by the Altiarchaea CRISPR system (Fig. 1A). To this end, we annotated genes of *Ca.* H. crystalense targeted by *Ca.* A. crystalense's CRISPR type I-B system and identified several hypothetical proteins, proteins lacking annotation, and non-coding genomic regions (these categories sum up to 98.25%). Targeted genes included a CTP synthase and a DNA methyltransferase N-4/N-6 domain protein (Fig. 2C, Table S5). Methyltransferases protect DNA against cleavage by restriction enzymes[35]. Inactivation of such a methyltransferase might increase vulnerability of the episymbiont towards enzymatic cleavage by the host.

CRISPR targeting in two independent host-episymbiont systems

Targeting of episymbiont's genomes by altiarchaeal CRISPR spacers was also observed in the HURL ecosystem. In contrast to *Ca.* A. crystalense's CRISPR-Cas I-B dependent targeting of *Ca.* H. crystalense genomes in the CG environment, *Ca.* Altiarchaeum horonobense found within the HURL ecosystem appeared to employ CRISPR spacers of an unassigned array (*i.e.*, no *cas* genes in direct vicinity could be detected due to genome fragmentation but the DR sequence is identical to type III CRISPR-Cas systems of other Altiarchaea[28]) to potentially ward off *Ca.* Huberiarchaeum julieae episymbionts and viral invaders (Fig. 1D). While spacers of this unassigned array targeting the *Ca.* H. julieae's genome exhibited greater diversity compared to the self-targeting counterparts of *Ca.* A. horonobense's (Fig. 1D), their relative abundance in the metagenome was nearly two-fold lower (Fig. 1E). The ecosystem-specific involvement of CRISPR-Cas I-B along with the unassigned array targeting of the episymbiont genomes in two distinct subsurface ecosystems seemingly indicates an independent evolution of defense against intruding DNA, which aligns with previous investigations that demonstrated a strict biogeography of *Ca.* Altiarchaea core genomes and site-specific evolution[36]. Given the site-specific evolution of *Ca.* Altiarchaea an alternative explanation for the acquisition of spacers against foreign chromosomal DNA might be avoidance of spoilage of the host chromosome by intruding genes (horizontal gene transfer). In Haloarchaea, such a mechanism has been shown to indirectly control for unwanted horizontal gene transfer between strains of the same genus[37].

Spacers of the unassigned CRISPR array were detected in much greater diversity than those of CRISPR I-B systems at the HURL site (Fig. 1D-E). While spacers of the unassigned array of CG-derived *Ca.* A. crystalense self-target chromosomal gene sequences, the spacers of the unassigned array of *Ca.* A. horonobense's self-target intergenic regions (Fig. 1C, Table S7). Notably, it has been demonstrated in haloarchaea that self-targeting does not necessarily lead to cell suicide[38]. Assuming that the CRISPR-Cas interference is associated with a defense against the symbiont, a plethora of spacers present at CG might effectively repress the symbiont (host:symbiont = 11:1 based on metagenomic read mapping), while a lower abundance of spacers targeting *Ca.* H. julieae at HURL was associated with a higher presence of episymbionts (host:symbiont = 6:1).

Episymbionts metabolically complement self-targeted hosts

We applied genome-scale metabolic modeling to examine the different symbiotic interactions of *Ca.* Altiarchaea and *Ca.* Huberiarchaea implicated by variations in the CRISPR systems and host-symbiont ratios of the two ecosystems analyzed. MAGs (ten genomes of *Ca.* A. crystalense, ten of *Ca.* H. crystalense, one of *Ca.* A. horonobense, one of *Ca.* H. julieae), SAGs (seven of *Ca.* A. crystalense and one of *Ca.* H. crystalense) and transcriptomic data (extracted spacers of samples CG05, CG08 and CG16 from 2015) from CG and HURL ecosystems were used to render genome-scale metabolic reconstructions. Although we applied thorough manual data curation[20,27], the genomes were fairly fragmented (average $N50_{host/CG}$ = 8067.24, average $N50_{symbtiont/CG}$ = 14983.73, average $N50_{host/HURL}$ = 3604, average $N50_{symbtiont/HURL}$ = 4115), and missing information due to fragmentation or binning errors cannot be excluded.

A consensus model was created for each ecosystem to cogently summarize and compare the metabolic capacities of *Ca.* Altiarchaeum and *Ca.* Huberiarchaeum, and constraint-based modeling of these metabolic networks facilitated an assessment of host-symbiont metabolic complementarity (Fig. 2E-F, Fig. S8). Models of the CG and HURL environment both revealed a significant reliance of *Ca.* Huberiarchaea upon its host's metabolism yet little to no dependency of the host upon the metabolism of *Ca.* Huberiarchaea. For example, glucose, amino acids, vitamins, and energy carrying compounds like adenosine triphosphate (ATP) were transferred from *Ca.* Altiarchaeum to *Ca.* Huberiarchaeum in both models (Table S8-S11; details in Supplementary Results), supporting the notion that *Ca.* Altiarchaeum is a primary producer, while *Ca.* Huberiarchaeum relies on its host for carbon and energy sources[14].

Analyses of CG and HURL host-symbiont relationships also revealed highly variable metabolic collaborations between episymbionts and their hosts. In the CG ecosystem, a deoxycytidylate monophosphate (dCMP) deaminase was absent in *Ca.* A. crystalense but present in *Ca.* H. crystalense. This gene is essential to reach a non-zero biomass for *Ca. A.* crystalense in the model (see Supplementary Results), suggesting a collaborative effort of synthesizing pyrimidine (Fig. S8C). Similarly, HURL-borne *Ca.* A. horonobense genomes lacked deoxythymidine monophosphate (dTMP) synthase genes, while these genes were present in the genomes of *Ca.* H. julieae – once again implicating collaboration, namely in folate biosynthesis (Fig. S8C; Fig. 3).

At HURL, the self-targeting of genes in *Ca.* Altiarchaea did not impact the host's dependency on the symbiont's metabolism within both CRISPR systems (Fig. S8, Supplementary Results). At CG, however, eliminating the functions of genes self-targeted by the I-B system in metabolic models exposed additional modes of complementing *Ca.* A. crystalense's metabolic demands by *Ca.* Huberarchaea via lysyl-tRNA synthetases and phenylalanyl-tRNA synthetases (Fig. 2D-E, Fig. 3, and Fig. S8A, and C-F). The respective protein sequences were not horizontally transferred between *Ca.* Altiarchaea and *Ca.* Huberiarchaea based on phylogenetic analyses; instead, the phenylalanyl-tRNA synthetase of *Ca.* Huberiarchaeum can be traced back with strong confidence to *Ca.* Woesarcheaota and *Ca.* Pacearchaeota (Supplementary Data).

While the protospacers of *Ca.* Altiarchaea viruses and *Ca.* H. crystalense harbored a definitive PAM (5'-TTN-3'associated with other I-B systems[39]), no such clear motif was detected in the host protospacers. Here, the second base of the putative PAM region, exhibited a four-fold greater than the average single nucleotide polymorphism (SNP) rate of genes (Fig. S9; details in Supplementary Results). Mutations in the PAM region diverging from the 5'-TTN-3' motif would prevent self-targeting at least for parts of the altiarchaeal population[40] and thus protect the host chromosome from CRISPR-Cas-mediated cleavage. In our model, removal of self-targeting would lessen the metabolic dependence on the symbiont and enable subpopulations of *Ca.* Altiarchaea to flourish more independently. The missing PAM sequence for self-targeting spacers and the increased SNP-rate in such regions compared to those targeting the episymbiont suggest that the population of *Ca.* Altiarchaea is adapting to escape the dependency of the symbiont. Considering that acquisition of self-targeting spacers is a stochastic process[41], escape mutations or deletions within the essential targeted genes could have detrimental effects on the cell viability due to the deficits in the corresponding metabolic activities resulting in cell suicide (reviewed in Heussler and O'Toole, 2016)[31]. Episymbionts could provide a temporary relief to the host cell by complementing the metabolic deficiency, becoming a bona fide symbiont, at least until the metabolic autonomy of the host is reestablished. We thus hypothesize that interactions between hosts and episymbiont depend on the genotype of the host and can consequently be either mutualistic or parasitic. However, cultivation of the host-symbiont system along with establishing a genetic system to modify the host genome are necessary to test this hypothesis.

Inter-phylum interactions in other symbiotic archaea

To facilitate the overlay of our findings on other potential archaeal host-DPANN episymbiont relationships, we analyzed CRISPR spacer matches between all archaeal genomes publicly available in NCBI's GenBank (7,012 genomes: state May, 2021, Table S4). After having extracted 106,641 spacer sequences, 39,875 distinct spacer-to-protospacer matches across all genomes were detected. Few contigs carrying CRISPR arrays (*e.g.,* for *Ca.* Micrarchaeum) also contained taxonomic hallmark genes, such as those coding for DNA-directed RNA polymerase subunit or ribosomal proteins, which provided additional confidence for the correct assignment of spacers to the fragmented public MAGs. The spacer hits accounted for both self-targeting and interspecies spacer interactions (Extended Data Fig. 4). Network analyses showed the genomes of the DPANN *Ca.* Aenigmarchaeota and *Ca.* Altiarchaeota (Fig. 4), as well as *Sulfolobus*, *Methanosarcina, Haloferax,* and *Halobacterium* spp. forming large clusters resulting from a wealth of interspecies hits and/or self-targeting (Extended Data Fig. 4), which was also previously shown for other archaea[37,42]. Well-established DPANN-host co-cultures, *e.g. Ignicoccus hospitalis* and *Nanoarchaeum equitans*[43], did not exhibit CRISPR-Cas-derived targeting to either of the symbionts in our archaeal genome dataset.

Particularly for the hydrothermal system of Guaymas Basin, Gulf of California[44], our approach enabled the *a priori* prediction of DPANN-host interactions based on CRISPR-Cas genome targeting (Fig. 4). Analyses of the spacer-protospacer matches from the read data of Guaymas Basin revealed frequent targeting (160 spacer-protospacer matches) of *Ca.* Aenigmarchaeota by *Ca.* Bathyarchaeota. Genes targeted by these spacer-protospacer matches, *e.g.,* encode for the LamGL domain-containing protein, which is *inter alia* responsible for the binding of sulfated glycolipids[45,46], and the ribonucleoside triphosphate reductase, amenable for catalysis of the conversion of ribonucleotides into deoxyribonucleotides[47].

Another host-DPANN interaction unveiled by these analyses involves *Ca.* Micrarchaeota spacers matching a Thermoprotei archaeon, with both of these genomes arising from the same ecosystem but a few centimeters apart in depth[44]. Comparing those targeted gene-encoding regions to the targeted genetic regions in *Ca.* Huberiarchaeum by spacers of *Ca.* Altiarchaeum (CTP synthase and DNA methylase, see above), no acquisition pattern of spacers directed against

genomic regions that encode specific functions could be detected. Overall, these findings suggest spacer-protospacer matches are a useful tool for identifying *in-silico* host-symbiont interactions of uncultivated archaea based on metagenomic analyses.

DISCUSSION

The findings discussed here demonstrate that archaeal CRISPR-Cas systems acquire resistance not only to genomes of foreign MGEs[1] and closely related species[32] but also to archaea of other phyla, particularly episymbionts belonging to the DPANN superphylum. Our results suggest that CRISPR-Cas-mediated adaptive immunity might lead to complex interactions between the host and symbiont at the population level, possibly drawing the host into maintaining a collaborative relationship with the symbiont due to balancing the self-targeting nature of the host's CRISPR system and the potential defense against the episymbiont. Based on our results from single-cell genomic data, metagenomes, and metatranscriptomes, we suggest that a double-edged sword drives the evolution of microbial populations, *i.e.*, CRISPR-Cas-mediated defenses likely render a major fraction of the DPANN episymbiont population truly parasitic, while the remainder seem to support the host in a mutualistic fashion.

Future studies should be set out with the aim of cultivating of the host-symbiont system to validate the herein proposed CRISPR-Cas interference. However, cultivation attempts might selectively enrich for systems with mutualistic relationship, and *in silico* screening of currently existing host-DPANN co-cultures for spacer targeting of the episymbiont's genome were devoid of such an interaction, including the well-known archaeal system *Ignicoccus hospitalis* and *Nanoarchaeum equitans*[13]. Consequently, genetic engineering of the host and the symbiont will be necessary to eventually clarify the relationship between hosts and DPANN symbionts – may it be mutualistic, parasitic, or a mixed population model as suggested by our findings.

METHODS

RNA extraction and metatranscriptomic sequencing. Samples for transcriptomics were collected along with DNA samples as previously published[20]. For the samples CG05, CG08 and CG16 we filtered approx. 189, 151, and 151 L of geyser-erupted water, respectively. The MoBio PowerMax

Soil DNA kit, now re-branded as the Qiagen DNeasy PowerMax Soil kit (Qiagen, Germantown, MD), was used to perform all metagenomic RNA extractions. Filters were aseptically cut into pieces, and 20 mL of lysis buffer from the kit was added for removal of cells from the filters. The manufacturer's alternative protocol, entitled "Alternative PowerMax Protocol for Isolation of RNA and DNA from Low Biomass Soil with Low Humics" was adjusted as follows: briefly, 10 mL of Bead Solution was added to the thawed filter and vortexed at maximum speed for 5 minutes to remove cells. The cell solution was transferred to a bead tube, and 5 ml of phenol:chloroform:isoamyl alcohol (25:24:1), pH 6.6, was added and homogenized by vortexing for 10 minutes. The manufacturer's protocol was followed thereafter. The metagenomic RNA extracts underwent DNase treatment using the Qiagen DNase Max kit (Qiagen), following manufacturer's standard protocol. Quality control and quantification of all RNA extracts were performed using the Agilent Bioanalyzer RNA 6000 Nano kit (Agilent, Santa Clara, CA). Sequencing libraries were created using the Illumina TruSeq Stranded mRNA Library Prep Kit, following manufacturer's protocol (Illumina, San Diego, CA). Libraries were sequenced on the Illumina HiSeq 2500 platform (Illumina).

Sample preparation for FISH. Groundwater for FISH analysis was sampled to visualize the Altiarchaea-Huberarchaea relationship within the CG and HURL ecosystem. Water from CG was sampled onto a 0.2 µm filter with a syringe filter holder until the filter started clogging and afterwards fixed by slowly pressing 3% formaldehyde (Thermo Fisher Scientific, MA, USA) through the filter to exchange the sample water with fixative. Fixation was performed for one hour in the dark. Within the filter holder, a washing step with 3x 20 mL Phosphate Buffered Saline (PBS) (conc. 1 v/v%) was done, followed by alternating washing and incubation with ethanol with 50, 70 and 100% (v/v)% for 10 minutes at room temperature. The filter holder was opened in a sterile environment, and the filter was stored in a petri dish with the biofilm facing upwards and then air dried for 10 minutes. Filter samples for FISH from CG of the sampling campaign in 2021 were covered and stored in RNA*later*™ (Invitrogen by Thermo Fisher Scientific; Ref: AM7021).

Imaging of FISH samples. FISH was performed according to Schwank et al.[14] with the following modifications. DAPI (4',6-Diamidino-2-Phenylindole) was used at concentrations of 4 µg per mL without dilution in the washing buffer. Visualization was performed with an Axio Imager M2m

epifluorescence microscope (X-Cite XYLIS Broad Spectrum LED Illumination System, Excelitas) equipped with an Axio Cam MRm and a Zen 3.4 Pro software (version 3.4.91.00000) (Carl Zeiss Microscopy GmbH, Jena, Germany). Imaging was carried out by using the 110x/1.3 oil objective EC-Plan NEOFLUAR (Carl Zeiss Microscopy GmbH) and three different filter sets (Carl Zeiss): 49 DAPI for imaging *Ca.* A. crystalense/horonobense cells and *Ca.* H. crystalense/julieae cells, 43 Cy3 for the detection of *Ca.* Huberiarchaea signals, and 09 for achieving 16S rRNA signals of *Ca.* Altiarchaea. The FISH images are shared within a Figshare folder (10.6084/m9.figshare.22739849).

Metagenome assembly and genome reconstruction. Omic datasets generated from sampling campaigns for CG[20,27] (Utah, USA) and HURL[24] (Japan) were downloaded from the NCBI Sequence Read Archive (SRA) in April 2019. Please refer to Table S1 (metagenomic and metatranscriptomic datasets), Table S2 (genome accessions of *Ca.* Aliarchaeum and *Ca.* Huberiarchaeum), and Table S3 (single cell genomic dataset) for all accession numbers of publicly available datasets and generated genomes used in this study. For all metagenomic datasets of CG and HURL, quality filtering and trimming of reads was done using BBduk (https://github.com/BioInfoTools/BBMap/blob/master/sh/bbduk.sh, version 37.09) and Sickle[48] (version 1.33). The MetaSPAdes[49] (version 3.10) and Bowtie2[50] utilities (--sensitive, version 2.3.5.1) were applied to assemble reads and estimate coverage, respectively. Scaffolds < 1 kbp were excluded from further analysis. The interactive uBin[51] software (version 0.9.14) was used to segregate the genomes of *Ca.* Altiarchaeum horonobense and *Ca.* Huberiarchaeum julieae based on %GC content, taxonomy, and coverage information. To determine genome completeness and contamination we used checkM[52] (v1.2.2) (Table S2). Previously published *Ca.* Huberiarchaeum genomes generated from each of the CG and HURL ecosystems were used as probes to identify respective scaffolds at the protein level (≥80% similarity).

Phylogeny of Altiarchaeum and Huberiarchaeum. A reference dataset spanning the diversity of 176 archaeal genomes was used to place *Ca.* Huberiarchaea and *Ca.* Altiarchaea phylogenetically. The accession numbers of all genomes within the reference datasets can be found in the Supplementary Data within the phylogenetic tree (with the suffix “GCA_”). To avoid redundancy, all genomes annotated as *Ca.* Altiarchaea on NCBI (June 2019), previously published *Ca.*

Altiarchaea genomes[36], and one representative genome from *Ca.* Altiarchaeum and *Ca.* Huberiarchaeum were consolidated for this work. Individual homology searches were executed across these datasets, using HMMER 3.2.1[53] with the Phylosift[54] marker HMM profiles and an e-value cutoff of 1 x 10^{-5}. All DNA sequences were aligned with MUSCLE v3.8.31[55] (default parameters) and manually curated to fuse fragmented genes and remove distant homologs and paralogous copies. One *Ca.* Altiarchaea genome (GCA_003663105) was likely contaminated and thus removed from the final alignments. Sequence sets resulting from each of the four datasets were fused together (36 single-gene datasets; one of the 37 Phylosift marker genes (DNGNGWU00035) was omitted due to many missing taxa), realigned as before, trimmed with BMGE (BLOSUM30)[56], and concatenated into one supermatrix (200 taxa; 5,974 amino acid positions). Phylogenies were reconstructed with IQ-TREE 2[57] (v2.0.5), first using ModelFinder[58], then using that phylogeny as a guide, with the PMSF model[59] (LG+C60+F+G). Branch supports were calculated using 1,000 ultrafast bootstrap[60] and 1,000 SH-aLRT[61] replicates and the aBayes[62] test and trees were visualized in iTOL[63] (version 5).

Naming of archaeal genomes. Except for *Ca.* Huberiarchaeum crystalense, all host and episymbiont species were previously only classified at the genus level or – in case of the episymbiont from the HURL ecosystem – not classified at all. Using established average nucleotide identity (ANI) and Average Amino Acid Identity (AAI) cutoffs along with phylogenetic analyses (Fig. 1 and Supplementary Data), we established the host-symbiont pairs as *Ca.* Altiarchaeum crystalense and *Ca.* Huberiarchaeum crystalense from the CG ecosystem (named after the ecosystem Crystal Geyser) and *Ca.* Altiarchaeum horonobense (named after the sampling site Horonobe) and *Ca.* Huberiarchaeum julieae (named after subsurface microbiologist Julie Huber).

Phylogenetic reconstruction of individual metabolic genes. For the phylogenies of lysine and phenylalanine (subunit B) tRNA synthetases, the protein sequences inferred from both genes from *Ca.* Altiarchaeum hamiconexum and *Ca.* Huberiarchaeum crystalense were used for homology searches against local databases of 1808 archaeal and 25118 bacterial genomes (all genomes of the respective domain on NCBI as of 2019.06.01 dereplicated at species level) with DIAMOND v2.0.15.153[64]. The maximum number of target sequences (-k 400) was determined by

trying different numbers (100, 200, 400, 800, 1000, 0/all), aligning with MAFFT FFT-NS-2 (v7.505) and running a preliminary phylogeny (BioNJ or PhyML without tree topology optimization) in Seaview version 5.0.4[65]. We picked the number that we deemed to give a reasonable view of the origin of each sequence, without including too many divergent homologs or increasing the downstream computational load too much. The original query sequences were added to the set of hits and aligned with MAFFT E-INS-I. The datasets were curated semi-manually (https://github.com/ProbstLab/Adam_Kolyfetis_2021_methanogenesis/blob/master/fuse_sequences.py) to fuse fragmented sequences, realigned as before, and trimmed with BMGE[56] (BLOSUM30). Phylogenies were reconstructed with IQ-TREE 2[57] using ModelFinder[58] for the model selection and branch supports calculated using 1000 ultrafast bootstrap[60] and 1000 SH-aLRT replicates.

CRISPR system extraction and viral sequence determination. The CRISPR systems of 18 distinct *Ca.* Altiarchaeum crystalense genomes[20,26] (Table S2) and one *Ca.* Altiarchaeum horonobense genome[24] (Table S2) were extracted with CRISPRCasFinder[66] (version 1.2), and annotated *cas* genes were used to identify CRISPR-Cas cassettes. Two resulting consensus DR sequences were used as input for MetaCRAST[67] (-d 1 -c 1 -a 1 -h -r), analysis of metagenomic reads, metatranscriptomic reads, and single cell genome reads. Only spacers having adjacent repeat sequences bearing 100% similarity with the respective read were considered. All spacers shorter than 24 bps, longer than 57 bps, or harboring homopolymers of six or more identical bases in a row were excluded. Spacers were clustered to 97% nucleotide identity using CD-hit[68] (version 4.8.1) and respective centroid sequences were used in downstream analyses.

To check if spacers were biased towards matching genome transcripts, the orientation of the CRISPR array was confirmed on all available *Ca*. Altiarchaeum crystalense genomes to identify the forward strand that corresponds to CRISPR-RNA by using CRISPRDirection2.0 with default settings[69]. To avoid false positive predictions of self-targeting and episymbiont targeting, we masked prophage region, predicted by VirSorter[70] (category 1-3, 4-6) and transposon regions, predicted by ISEScan[71]. The spacers from this analysis were blasted (nucleotide blast, bidirectional [default setting] and unidirectional [-strand plus] on the forward strand) against the CDS data of 18 *Ca.* Altiarchaeum crystalense genomes (including seven SAGs), eleven *Ca.*

Huberiarchaeum crystalense (including 2 SAGs), one genome of *Ca.* Altiarchaeum horonobense and *Ca.* Huberiarchaeum julieae, respectively. All unpublished viral genomes used in this study are deposited in the Figshare folder (10.6084/m9.figshare.22738568).

Detection, dereplication and analysis of DNA viral scaffolds. Assembled metagenomes were used to extract and predict viral and putatively viral sequences as previously performed[28]. In brief, predicted viral operational taxonomic units (vOTUs) >3kb were dereplicated via usearch[72] at 95% nucleotide identity resulting in centroid sequences for downstream analysis. VOTUs were identified via blastn[73] (--short, filtering for 80% similarity, version 2.9.0+) of Clustered regularly interspaced short palindromic repeat (CRISPR)-derived spacers against centroid vOTUs. Completeness and origin (host, viral, unclassified) of vOTUs was assessed using CheckV v.0.4.0[74]. Clustering of viral sequences with a recent viral Refseq database[75] (release July 2022). and previously detected Altiarchaea-targeting viruses[28] was performed using vConTACT2[76,77] v.0.11.3, VICTOR[78] (using nucleic acid sequences) and VIRIDIC[79] under default settings and for calculating intergenomic similarities. In VICTOR, all pairwise comparisons of the nucleotide sequences were conducted using the Genome-BLAST Distance Phylogeny[80] (GBDP) method under settings recommended for prokaryotic viruses[78]. The resulting intergenomic distances from VICTOR were used to infer a balanced minimum evolution tree with branch support via FastME including Subtree Pruning and Regrafting post-processing[81] for the distance formula D0. Branch support was inferred from 100 pseudo-bootstrap replicates each. Trees were rooted at the midpoint[82]. Visualization of viral clusters identified with vConTACT2 in conjunction with the viral RefSeq database was performed using Cytoscape v.3.9.02[83]. In addition, a circular proteomic tree with viral genomes using the Virus-Host DB: RefSeq release 217 was build using ViPTree version 3.5.[84] . Within ViPTree, dsDNA was selected as nucleic acid type and “any host” chosen as host category.

Sliding window for coverage analysis of regions targeted by CRISPR spacers. Variations in coverage over the genomes were investigated to deduce possible negative selection at targeted sites. Targeted scaffolds from individual genomes were mapped back to the raw reads (from sample CG05, CG08 and CG16) with Bowtie2[50] with default settings. Mappings were filtered to remove hits with more than three mismatches using SAMtools[85] (version 1.10). Genomecov from

BEDtools (version 2.27.1) was used to calculate coverage per position[86]. The first and last 150 base pairs of each scaffold, and possible transposons and viruses were masked by setting the breadth to zero. Mean breadth from sliding windows of 35 base pairs were calculated. In addition, all position with a coverage lower than 10 were excluded. The median coverage of each scaffold (δ) serves to differentiate high and low breadth. Wilcoxon signed rank tests (standard function R[87]) were performed between targeted regions of a scaffold and the same amount of randomly drawn non-targeted windows from the same scaffold. Random sampling and the test were repeated 1000 times for each scaffold.

Models for *Ca.* Altiarchaea and *Ca.* Huberarchaea host-symbiont interaction based on genomic information. To infer metabolic interactions, genome-scale metabolic reconstructions of *Ca.* Altiarchaeum crystalense/horonobense and *Ca.* Huberiarchaeum crystalense/julieae (see accession numbers Table S2) were based on MAGs and SAGs identified from CG (AltiCG-HuberCG model) and HURL (AltiHURL-HuberHURL model). The genome-scale metabolic models of AltiCG-HuberCG and AltiHURL-HuberHURL were represented in a YAML format following conventions defined by the PSAMM software package[89,90]. The AltiCG-HuberCG model included 515 genes of *Ca.* A. crystalense and 88 genes of *Ca.* H. crystalense, associated with 477 and 125 reactions, respectively (Table S8). The AltiHURL-HuberHURL model included 388 *Ca.* A. horonobense and 78 *Ca.* H. julieae genes, associated with 495 and 128 reactions, respectively (Table S9). Each model contained two compartments (one for *Ca.* Altiarchaeum and one for *Ca.* Huberiarchaeum), with either restricted or unlimited metabolite exchanges between the two compartments to model the metabolite availability upon cytoplasmic fusion of the two organisms.

Details of the model are represented in Tables S8 - S11. The CG model was based on the prediction of metabolic pathways using combined annotation of all MAGs and SAGs identified from this and a prior study[14]. Protein sequences annotated from the individual MAGs and SAGs were clustered at 100% amino acid identity using CD-HIT[68,91], followed by a pangenome analysis to capture metabolic capacities represented by the entire population. Automated metabolic reconstruction was performed based on ortholog mapping to (i) existing models of other archaeal strains, i.e. *Pyrococcus furiosus*, *Thermococcus eurythermalis*, *Methanosarcina barkeri* and *Methanococcus maripaludis*[92,93], and (ii) public databases, such as the Kyoto Encyclopedia of

Genes and Genomes[94] (KEGG), EggNOG[95] and Transporter Classification Database[96] (TCDB). Extensive manual curations were carried out following the automated reconstruction to integrate prior annotations of *Ca.* Altiarchaeum's and *Ca.* Huberiarchaeum's metabolism[14,20], as well as latest biochemical evidence of enzymatic functions in archaeal organisms (Tables S8 and S9). Overall, literature evidence was assigned to 137 reactions in the model for AltiCG-HuberCG and 144 reactions in the model for AltiHURL-HuberHURL through homologous mapping to experimentally verified enzymes. The biomass equations of *Ca.* Altiarchaeum and *Ca.* Huberiarchaeum were individually formulated in both models following a standard procedure (Table S8 and S9). The biosynthesis of macromolecules (e.g., DNA, RNA, protein, and lipids) were defined to account for the mM composition of each building block in assembling 1 g of a given component and the associated energy cost. The stoichiometry of DNA and RNA biosynthesis was derived based on the average composition of nucleotides in the genomes and coding genes, respectively. The energy cost for DNA and RNA synthesis was estimated as 2 mM of ATP per millimole of nucleotides according to the mechanism of polynucleotide biosynthesis[97]. The stoichiometry of protein biosynthesis was calculated based on the average composition of amino acids in the corresponding proteome, and the associated energy cost was estimated based on the mechanism of protein synthesis[98], where one ATP was consumed for each tRNA charging, and two GTPs were consumed for extending one amino acid to a growing peptide chain. The tRNA charging equations were represented separately for each amino acid. The stoichiometry of lipid biosynthesis was formulated based on experimental measurements of the weight compositions of core lipids and header groups of *Ca.* Altiarchaeum or *Ca.* Huberiarchaeum of the respective system[20]. Following the definition of macromolecular synthesis functions, the biomass equations of *Ca.* A. crystalense, *Ca.* H. crystalense, *Ca.* A. horonobense, and *Ca.* H. julieae were formulated to represent the gram composition of DNA, RNA, proteins, lipids, and vitamins in 1 g of cell dry weight (gDW). Relative abundance (based on coverage) of the respective genomes was calculated via metagenomic read mapping with Bowtie2[50] (--sensitive mode). The CG- and HURL-specific *Ca.* Altiarchaeum and *Ca.* Huberiarchaeum biomass were then combined based on an estimation of their relative abundance in the respective ecosystems using the metagenomic data. Specifically, the combined Altiarchaeum-Huberiarchaeum biomass has a relative

Huberiarchaeum:Altiarchaeum ratio between 0.06 and 0.12 in the CG system, and a ratio of 0.205 in the HURL system (as estimated via stringent read mapping, see Supplementary Results).

Metabolic modeling and reconstruction. Consensus models of *Ca.* Altiarchaeum to *Ca.* Huberiarchaeum were constructed based on collections of MAGs and SAGs from CG (20 MAGs, 8 SAGs) and HURL (2 MAGs) (Table S2) to capture the metabolic potential of each population. Candidate genes were first identified based on a pangenome analysis, which was performed following ortholog identification using a bidirectional best hit approach[88]. All representative genes from the MAGs or SAGs of a given ecosystem served as candidates for that ecosystem's metabolic reconstruction. Complementary metabolic characteristics were identified between *Ca.* Altiarchaeum and *Ca.* Huberiarchaeum via a *fastgapfill* implementation in the PSAMM software (version v1.0) package[89,90] using the cplex solver (v12.7.1.0). Simulations targeted the growth optimization of *Ca.* Altiarchaeum while applying the metabolic reactions of *Ca.* Huberiarchaeum as a reference, which facilitated the identification of *Ca.* Huberiarchaeum-encoded complementary functions essential for *Ca.* Altiarchaeum - and vice versa. Combined *Ca.* Altiarchaeum and *Ca.* Huberiarchaeum metabolic models were formulated with exchange constraints representative of environmental *in situ* geochemical measurements corresponding to either CG or HURL (Table S9 and S10). Comparative analyses based on computational simulations were carried out in the presence or absence of CRISPR-targeted genes. This enabled the identification of changes in metabolite transfer and/or metabolic collaboration between *Ca.* Altiarchaeum and *Ca.* Huberiarchaeum (Fig. S8) upon targeting specific genes with spacers. Metabolic gaps in the production of biomass components by *Ca.* Altiarchaea were identified using the PSAMM *fluxcheck* and *gapcheck* functions[89,90] Candidate gap-filling reactions for unblocking each biomass component were identified using the PSAMM *fastgapfill* implementation with the KEGG reaction database[94] as a reference, and subsequently curated before being incorporated into the models. A total of 17 gap-filling reactions were included in the *Ca.* Altiarchaea compartment of both CG and HURL models, including functions in the citrate cycle, amino acids-, lipids-, and cofactor-biosynthesis. The overall stoichiometric consistency, formula and charge balance of the model were validated using the PSAMM *masscheck*, *formulacheck*, and *chargecheck* functions[89,90]. The exchange reactions, compound sources or sinks, biomass

equations and reactions involving compounds with undefined group R or X were excluded from formula and charge checks but instead manually inspected to ensure proper formulation.

Metabolic simulations were performed with PSAMM version 1.0 using the IBM ILOG CPLEX Optimizer version 12.7.1.0 (https://www.ibm.com/products/ilog-cplex-optimization-studio). Simulation of the *Ca.* Altiarchaeum – *Ca.* Huberiarchaeum metabolism was formulated with exchange constraints that represent the corresponding *in situ* geochemical measurements in the CG[20] and HURL[24]. These geochemical measurements included the ion concentrations in porewater and the compositions of headspace gas (Table S8 - S11). Some measurements, e.g., CO_2 and H_2 at the CG site, were not available, but the compounds were required for biomass production in the *Ca.* Altiarchaeum – *Ca.* Huberiarchaeum system, and thus they were added to the exchange without implicit constraints. To simulate the fusion of the cytoplasm between *Ca.* Altiarchaeum and *Ca.* Huberiarchaeum, unlimited metabolite exchange was introduced to allow the free transfer of all small-molecular metabolites (excluding macromolecules, such as DNA, RNA, protein, lipids, and biomass) between the *Ca.* Altiarchaeum and *Ca.* Huberiarchaeum cell compartments.

To identify complementary metabolic processes between *Ca.* Altiarchaea and *Ca.* Huberiarchaea, the PSAMM *fastgapfill* implementation[89,90] was applied to optimize the *Ca.* Altiarchaea biomass while using all metabolic reactions in the *Ca.* Huberiarchaea compartment as a reference database, and vice versa, using corresponding models for CG or HURL. A list of metabolic reactions, including metabolite exchange functions between *Ca.* Altiarchaea and *Ca.* Huberiarchaea, was identified from this automated gap filling procedure to reveal the potential metabolic interactions between the two archaea at each site. The predicted complementary metabolites were subsequently confirmed by showing that the removal of any metabolite exchange would lead to a non-viable *Ca.* Altiarchaea or *Ca.* Huberiarchaea (biomass production is zero), suggesting that these metabolite exchanges reflect minimal essential interactions between *Ca.* Altiarchaea and *Ca.* Huberiarchaea of a given site (Table S8 and S9). Genes corresponding to the CRISPR type I-B and the unassigned CRISPR array spacer targeting in both CG and HURL systems were mapped to the metabolic reconstructions of AltiCG-HuberCG and AltiHURL-HuberHURL, respectively, for the identification of putative targets for simulating the

metabolic influences of attacks targeted by the CRISPR system (Table S10 and S11). To identify changes in the *Ca.* Altiarachaea – *Ca.* Huberiarchaea metabolic collaboration when considering attacks of respective genes by CRISPR-Cas systems, comparisons were made between the exchange unlimited model (where all metabolites (with the exception of macromolecules) were allowed to transfer freely between *Ca.* Altiarchaeum and *Ca.* Huberiarchaeum) and the exchange limited model (where only the complementary metabolites were allowed to transfer between *Ca.* Altiarchaeum and *Ca.* Huberiarchaeum). Flux variability analysis (FVA) was applied to the optimization of the combined Altiarchaeum-Huberiarchaeum biomass in the limited or unlimited models. Pathways that are required for complementing the effect of CRISPR spacer attacks were identified by comparing the FVA results of the limited and unlimited models. If the deletion of a spacer attacked gene would result in a zero-biomass flux in the limited model while a non-zero biomass flux in the unlimited model, a complementary pathway to the corresponding gene deletion was explored by identifying the enabling functions in the unlimited model. Note that the FVA was performed in PSAMM using the CPLEX Optimizer version 12.7.1.0, a zero range is defined as any fluxes within $1E^{-6}$ from zero.

PAM analysis of *Ca.* Altiarchaea, *Ca.* Huberarchaea, and viruses. Applying CRISPRTarget[99] (accessed in June 2020) with default settings, protospacer adjacent motifs (PAMs) were identified within the genomes of *Ca*. Altiarchaea, *Ca.* Huberarchaea, and viruses using spacers bearing 80% sequence similarity. CRISPRTarget results were screened with WebLogo[100,101] (v2.8.2) in batches of 10,000 8-bps sequences.

SNP analysis. To identify *Ca.* Altiarchaeum crystalense SNPs, reads from samples CG05, CG08, and CG16 (samples for which also transcriptomic datasets were available, and which were used in the metabolic modeling) were aligned to nine different MAGs (Table S2) and analyzed individually by using BBMap (https://sourceforge.net/projects/bbmap/, version 38.92) (default parameters). SNPs were predicted using the VarScan[102] pileup2snp command (v2.4.3; default settings) with observations and coverage thresholds set to a minimum of two and eight, respectively. SNPs bearing the reference allele 'N' were excluded if all base called reads showed this 'N'.

Synthesis of *cas* genes derived from *Ca.* Altiarchaea MAGs. The CRISPR-Cas gene cassette (Cas1, Cas2, Cas3, Cas4, Cas5, Cas8b) of one single-cell amplified genomes (SAG) of *Ca.* Altiarchaeum was used in gene synthesis. The Cas6 gene was annotated in two other SAGs of *Ca.* Altiarchaea, once with 438 and 468 amino acids respectively. To synthesize these genes, the sequences were first codon optimized using the BOOST design software v.1.3.9[103] and an *E. coli* codon frequency table. The synthetic DNA fragments were obtained from Twist Bioscience, CA, USA, which were later PCR amplified and cloned into the NcoI and XhoI sites of the pET28b vector using the NEBuilder HiFi Assembly kit (E2621X, New England BioLabs). The PCR was performed using the KAPA HiFi HotStart ReadyMix (Roche Sequencing, Pleasanton, CA, USA) according to the manufacturer recommended cycling protocol. The sequences of the refactored *cas* genes were verified by Pacific Bioscience sequencing. The synthetic building blocks and PCR primer sequences are listed in Table S13.

CRISPR-Cas activity assay in TXTL. The activity of the *Ca.* Altiarchaea type I-B CRISPR-Cas system was tested in a cell-free transcription-translation (TXTL) system. Circular or linear DNA constructs that were added to a TXTL reaction were transcribed and translated, and RNAs and proteins were produced[104]. The reaction conditions of the TXTL reactions performed here were adapted from Wimmer et al.[29]. A deGFP reporter plasmid was generated with Site Directed Mutagenesis (SDM) using p70a_deGFP_PacI[29] as backbone and introducing a TTTTC motif 12 nucleotides upstream of the p70a promoter driving the deGFP expression. The TTTTC motif was used as a putative PAM sequence because this motif was found next to a sequence matching a type I-B spacer (see main text). Constructs encoding single spacer arrays driven by the constitutive promoter J23119 contained either a spacer targeting the p70a promoter region of the reporter plasmid or a non-targeting spacer. These constructs were generated by Golden Gate adding spacer sequences in a plasmid which contained two repeat sequences interspaced by two BbsI restriction sites. The construct p70a-T7RNAP[104] encoding the T7 RNA polymerase and Isopropyl β-D-1-thiogalactopyranoside (IPTG; Carl Roth, Karlsruhe, Germany) was added to the TXTL reaction to ensure expression of the *cas* genes. Two Master mixes containing plasmids encoding for Cascade-forming *cas* proteins were prepared using the stoichiometry Cas8b1-Cas77-Cas51-Cas61, namely one for the 245 and the 268 amino acids long Cas6. A volume of 3 µL TXTL reaction were prepared

in Costar 3357 96-well V-bottom plates (Corning, NY, USA) with Costar 2080 cover mats (Corning) using the liquid handling machine Echo525 (Beckman Coulter, Brea, CA, USA) including the following components: 2.25 µL myTXTL Sigma 70 MasterMix (Arbor Biosciences, MI, USA), 0.2 nM p70a-T7RNAP, 0.5 mM IPTG, 3 nM Cascade Master mix, 1 nM Cas3 plasmid, and 1 nM targeting or non-targeting spacer plasmid. After a 4 h pre-incubation period at 29°C to allow the ribonucleoprotein complex of Cascade and crRNA to form, 1 nM deGFP reporter plasmid containing the TTTTC motif was added to the TXTL reactions. The reactions were incubated at 29°C for additional 16 h while measuring deGFP expression with BioTek Synergy H1 plate reader (BioTek, Winooski, VT, USA) at 485/528 nm excitation/emission[105]. Targeting spacer-mediated binding of the Cascade complex to the target region in the deGFP driving promoter or target plasmid degradation by Cas3 would lead to inhibition of deGFP production. The non-targeting spacer does not affect deGFP production and was used as a control. The fluorescence background values were measured with reactions containing solely myTXTL Sigma 70 MasterMix and nuclease-free H_2O and were subtracted from the endpoint deGFP values of the TXTL reactions. Significance between deGFP values derived from the non-targeting and targeting samples was calculated with Welch's t-test. All results showed a p-value > 0.05 and were therefore seen as non-significant. Hence, we concluded that the type I-B systems do not exhibit binding or degradation activity under the tested conditions. This could be due to the conditions used here not reflecting the conditions at the sampling site of *Ca.* Altiarchaea, or the motif TTTTC being a non-recognized PAM. All reactions were performed in triplicates.

PAM assay in TXTL (PAM-DETECT). To reveal the PAM diversity recognized by the type I-B system of *Ca.* Altiarchaea, PAM-DETECT (PAM DETermination with Enrichment-based Cell-free TXTL) was performed. A detailed protocol can be found in Wimmer et al.[29]. A plasmid containing a PAM library of five randomized nucleotides was used as a target plasmid. A single spacer array plasmid is constructed as mentioned above harboring a spacer targeting the target plasmid adjacent to the randomized nucleotides. Upon recognition of a PAM sequence, the Cascade complex binds to its target and thereby covers a PacI recognition site included in the target region. Cascade-bound target plasmids are protected from PacI digestion leading to an enrichment of recognized PAMs, detected by next-generation-sequencing (NGS; specified below). Separate 6 µL TXTL

reactions were prepared containing one or the other Cascade Master mix mentioned above. TXTL reactions contained: 4.5 µL myTXTL Sigma 70 Master mix, 0.2 nM pET28a_T7RNAP[29], 0.5 mM IPTG, 3 nM Cascade Master mix, 1 nM targeting spacer plasmid (targeting PAM library plasmid) and 1 nM PAM library plasmid (pPAM_library)[29]. After incubation at 29°C for 16 h, the TXTL samples were diluted 1:400 in nuclease-free H_2O. A volume of 500 µL of the dilution was digested with 0.09 units μL^{-1} PacI (NEB) in 1x CutSmart Buffer (NEB) at 37°C for 1 h. A "non-digested" control was prepared using 500 µL of the dilution and adding nuclease-free H_2O instead of PacI. PacI was inactivated at 65°C for 20 min and proteins were digested with 0.05 mg mL^{-1} Proteinase K (Cytiva, Marlborough, MA, USA) at 45°C for 1 h. Proteinase K was inactivated at 95°C for 5 min and remaining plasmids were extracted with standard ethanol precipitation. To prepare sequencing libraries, Illumina adapters with unique dual indices were added in two amplifications steps using KAPA HiFi HotStart Library Amplification Kit (KAPA Biosystems, Wilmington, MA, USA) and purification by AMPure XP (Beckman Coulter) after every amplification step. A volume of 15 µL of the ethanol-purified samples was used in a 50 µL PCR reaction with 19 cycles to add Illumina sequencing primer sites. The flow cell binding sequence was added in the second PCR reaction using 1 ng purified amplicons generated with the first PCR in a 50 µL reaction and 18 cycles. NGS was performed on an Illumina NovaSeq 6000 sequencer with 50 bp paired-end reads and 2.0 million reads per sample. PAM wheels were generated according to Leenay et al.[106] and Ondov et al.[107] and are not depicted here as no PAM enrichment was observed. Absence of PAM enrichment might be due to the reaction conditions of PAM-DETECT deviating from the conditions at the sampling site of *Ca.* Altiarchaea. PAM-DETECT assays were performed in duplicates.

CRISPR-Cas interactions across archaeal diversity. All archaeal genomes housed in the publicly accessible NCBI database (May 2021; Table S4) were screened for viral sequence contaminants using VirSorter[70] (default settings), and all respective hits, as well as annotated plasmids, were excluded from consideration. The CRISPRCasFinder[66] (version 2.0.3) utility was used to extract spacers, DR, and *cas* genes from each genome individually with the help of the *cas* gene database (-ArchaCas). All CRISPR arrays detected were masked in their respective genomes to avoid false positives, and spacers were filtered for homopolymers and sequence length as described above.

All spacer sequences were queried[73] against all archaeal genomes to an 80% nucleotide similarity threshold, and interactions between genomes based on CRISPR spacer matches were visualized in Cytoscape[83] (version v.3.9.02). The taxonomy of each genome was pulled from the NCBI taxonomy database and in single cases validated using Genome Taxonomy Database[108–110](GTDB-Tk classify, version v0.3.3, database r89). To avoid false positive predictions of self-targeting and episymbiont targeting, we masked prophage region, predicted by VirSorter[70] (category 1-3, 4-6).

ACKNOWLEDGEMENTS

This effort was funded by the Ministerium für Kultur und Wissenschaft des Landes Nordrhein-Westfalen ("Nachwuchsgruppe Dr. Alexander Probst") and the German Science Foundation under project NOVAC (grant number DFG PR1603/2-1) and through SPP 2141 (grant number DFG BE6703/1-1). Genome-scale metabolic modeling was supported by the National Science Foundation under Grant No. 1553211. The Ministry of Economy, Trade and Industry of Japan funded a part of the work as "The project for validating assessment methodology in geological disposal system" (2019 FY, Grant Number: JPJ007597). The work (proposal: 10.46936/10.25585/60000800) conducted by the U.S. Department of Energy Joint Genome Institute (https://ror.org/04xm1d337), a DOE Office of Science User Facility, is supported by the Office of Science of the U.S. Department of Energy operated under Contract No. DE-AC02-05CH11231. M.P. is supported by the Austrian Science Funds (Project MAINTAIN, DOC 69 doc.funds). P.S.A was supported by a postdoctoral fellowship from the Alexander von Humboldt Foundation. J.P. was supported by Lundin Energy Norway AS within the framework of the GeneOil Project. J.R. was supported by the German Science Foundation (grant number RA3432/1-1, project number 446702140). Support by the German Federal Ministry of Education and Research within the project "MultiKulti" (BMBF funding code: 161L0285E) is acknowledged. We thank Ken Dreger for exemplary server administration, and Bettina Siebers, Ivan Berg, Jillian F. Banfield and Benjamin Meyer for insightful discussion.

CONFLICT OF INTEREST

The authors declare no conflict of interest.

AUTHOR CONTRIBUTIONS

SPE and AJP performed genome-resolved metagenomics, while SPE and JR performed viromics. JR analyzed viral genomes with input from MK. CRISPR-Cas analyses were done by SPE, JR and AJP. SNP analysis was performed by MP and TR. Genome-scale modeling was conducted by WZ and YZ with input from SPE, PAFG, and AJP. Phylogenomic analyses were carried out by PSA. TLVB provided bioinformatic assistance, and KSch and VT performed microscopy and initial metabolic analyses. JM and WB re-sampled Crystal Geyser and, JL, TW, and AJP conducted RNA extraction and sequencing, and SPE analyzed transcriptomes. FW and CB performed binding, cleavage and PAM assays and JL, JJ, YA, TW, and AJP generated/provided raw data. KS and SPE analyzed the archaeal CRISPRCas interactions from published NCBI archaeal genomes. AJP conceptualized the work. SPE, JR, WZ, YZ, and AJP wrote the manuscript with input from all authors.

DATA AVAILABILITY STATEMENT

Metagenomic datasets generated from the Crystal Geyser (CG)[20,27] ecosystem (Utah, USA) in 2009, 2014, and 2015 (n = 66), and the Horonobe Underground Research Laboratory (HURL)[24] (Hokkaido, Japan) environment (n = 2) were downloaded from the NCBI' Sequence Read Archive (SRA) in April 2019 (Table S1). SAGs generated in a previous study[20] (n = 219) were retrieved from the JGI's Integrated Microbial Genomes and Microbiomes database[111] (Table S3). The metagenome-derived genomes of *Ca.* A. crystalense and *Ca.* H. crystalense from CG are publicly accessible from NCBI (accession numbers in Table S2). The genomes of *Ca.* A. horonobense and *Ca.* H. julieae from HURL were newly reconstructed in this investigation (Table 2). All previously unpublished genomes used in this study are available in a Figshare folder 10.6084/m9.figshare.22339555 and all viral genomes are available here: 10.6084/m9.figshare.22738568.

CODE AVAILABILITY STATEMENT

The code used in this publication is based on previously published code. Please refer to the method section for information regarding the software and versions used.

REFERENCES

1. Garneau, J. E. *et al.* The CRISPR/Cas bacterial immune system cleaves bacteriophage and plasmid DNA. *Nature* **468**, 67 (2010).
2. Andersson, A. F. & Banfield, J. F. Virus population dynamics and acquired virus resistance in natural microbial communities. *Science* **320**, 1047–50 (2008).
3. Koonin, E. V. & Makarova, K. S. Evolutionary plasticity and functional versatility of CRISPR systems. *PLOS Biol.* **20**, e3001481 (2022).
4. Makarova, K. S. *et al.* An updated evolutionary classification of CRISPR–Cas systems. *Nat. Rev. Microbiol.* **13**, 722 (2015).
5. Makarova, K. S. *et al.* Evolutionary classification of CRISPR–Cas systems: a burst of class 2 and derived variants. *Nat. Rev. Microbiol.* **18**, 67–83 (2020).
6. Maniv, I., Jiang, W., Bikard, D. & Marraffini, L. A. Impact of different target sequences on type III CRISPR-Cas immunity. *J. Bacteriol.* **198**, 941 (2016).
7. Marraffini, L. A. & Sontheimer, E. J. Self versus non-self discrimination during CRISPR RNA-directed immunity. *Nature* **463**, 568–571 (2010).
8. Dombrowski, N., Lee, J.-H., Williams, T. A., Offre, P. & Spang, A. Genomic diversity, lifestyles and evolutionary origins of DPANN archaea. *FEMS Microbiol. Lett.* **366**, (2019).
9. Rinke, C. *et al.* Insights into the phylogeny and coding potential of microbial dark matter. *Nature* **499**, 431–437 (2013).
10. Castelle, C. J. *et al.* Biosynthetic capacity, metabolic variety and unusual biology in the CPR and DPANN radiations. *Nat. Rev. Microbiol.* **16**, 629–645 (2018).

11. Sakai, H. D. *et al.* Insight into the symbiotic lifestyle of DPANN archaea revealed by cultivation and genome analyses. *Proc. Natl. Acad. Sci.* **119**, e2115449119 (2022).
12. Jahn, U. *et al. Nanoarchaeum equitans* and *Ignicoccus hospitalis*: new insights into a unique, intimate association of two archaea. *J. Bacteriol.* **190**, 1743–1750 (2008).
13. Huber, H. *et al.* A new phylum of Archaea represented by a nanosized hyperthermophilic symbiont. *Nature* **417**, 63–67 (2002).
14. Schwank, K. *et al.* An archaeal symbiont-host association from the deep terrestrial subsurface. *ISME J.* **13**, 2135–2139 (2019).
15. Hamm, J. N. *et al.* Unexpected host dependency of Antarctic *Nanohaloarchaeota*. *Proc. Natl. Acad. Sci.* **116**, 14661 (2019).
16. Munson-McGee, J. H. *et al. Nanoarchaeota*, their *Sulfolobales* host, and *Nanoarchaeota* virus distribution across Yellowstone National Park hot springs. *Appl. Environ. Microbiol.* **81**, 7860–7868 (2015).
17. Jarett, J. K. *et al.* Single-cell genomics of co-sorted *Nanoarchaeota* suggests novel putative host associations and diversification of proteins involved in symbiosis. *Microbiome* **6**, 161 (2018).
18. Wurch, L. *et al.* Genomics-informed isolation and characterization of a symbiotic Nanoarchaeota system from a terrestrial geothermal environment. *Nat. Commun.* **7**, 12115 (2016).
19. Hamm, J. N. *et al.* The intracellular lifestyle of an archaeal symbiont. *bioRxiv* 2023.02.24.529834 (2023).

20. Probst, A. J. *et al.* Differential depth distribution of microbial function and putative symbionts through sediment-hosted aquifers in the deep terrestrial subsurface. *Nat. Microbiol.* **3**, 328–336 (2018).
21. Heimerl, T. *et al.* A complex endomembrane system in the archaeon *Ignicoccus hospitalis* tapped by *Nanoarchaeum equitans*. *Front. Microbiol.* **8**, 1072 (2017).
22. Comolli, L. R. & Banfield, J. F. Inter-species interconnections in acid mine drainage microbial communities. *Front. Microbiol.* **5**, 367 (2014).
23. Baker, B. J. *et al.* Enigmatic, ultrasmall, uncultivated Archaea. *Proc. Natl. Acad. Sci.* **107**, 8806–8811 (2010).
24. Hernsdorf, A. W. *et al.* Potential for microbial H_2 and metal transformations associated with novel bacteria and archaea in deep terrestrial subsurface sediments. *ISME J.* **11**, 1915–1929 (2017).
25. Probst, A. J. *et al.* Biology of a widespread uncultivated archaeon that contributes to carbon fixation in the subsurface. *Nat. Commun.* **5**, 5497 (2014).
26. Probst, A. J. *et al.* Genomic resolution of a cold subsurface aquifer community provides metabolic insights for novel microbes adapted to high CO_2 concentrations. **19**, 459–474 (2017).
27. Emerson, J. B., Thomas, B. C., Alvarez, W. & Banfield, J. F. Metagenomic analysis of a high carbon dioxide subsurface microbial community populated by chemolithoautotrophs and bacteria and archaea from candidate phyla. *Environ. Microbiol.* **18**, 1686–1703 (2016).
28. Rahlff, J. *et al.* Lytic archaeal viruses infect abundant primary producers in Earth's crust. *Nat. Commun.* **12**, 4642 (2021).

29. Wimmer, F., Mougiakos, I., Englert, F. & Beisel, C. L. Rapid cell-free characterization of multi-subunit CRISPR effectors and transposons. *Mol. Cell* **82**, 1210-1224.e6 (2022).
30. Marshall, R. *et al.* Rapid and scalable characterization of CRISPR technologies using an *E. coli* cell-free transcription-translation system. *Mol. Cell* **69**, 146-157.e3 (2018).
31. Heussler, G. E. & O'Toole, G. A. Friendly Fire: Biological functions and consequences of chromosomal targeting by CRISPR-Cas systems. *J. Bacteriol.* **198**, 1481–1486 (2016).
32. Stern, A., Keren, L., Wurtzel, O., Amitai, G. & Sorek, R. Self-targeting by CRISPR: gene regulation or autoimmunity? *Trends Genet.* **26**, 335–340 (2010).
33. Aklujkar, M. & Lovley, D. R. Interference with histidyl-tRNA synthetase by a CRISPR spacer sequence as a factor in the evolution of *Pelobacter carbinolicus*. *BMC Evol. Biol.* **10**, 230 (2010).
34. Bhaya, D., Davison, M. & Barrangou, R. CRISPR-Cas systems in Bacteria and Archaea: Versatile small RNAs for adaptive defense and regulation. *Annu. Rev. Genet.* **45**, 273–297 (2011).
35. Wilson, G. G. Organization of restriction-modification systems. *Nucleic Acids Res.* **19**, 2539–2566 (1991).
36. Bornemann, T. L. V. *et al.* Genetic diversity in terrestrial subsurface ecosystems impacted by geological degassing. *Nat. Commun.* **13**, 284 (2022).
37. Turgeman-Grott, I. *et al.* Pervasive acquisition of CRISPR memory driven by inter-species mating of archaea can limit gene transfer and influence speciation. *Nat. Microbiol.* **4**, 177–186 (2019).

38. Stachler, A.-E. *et al.* High tolerance to self-targeting of the genome by the endogenous CRISPR-Cas system in an archaeon. *Nucleic Acids Res.* **45**, 5208–5216 (2017).
39. Vink, J. N. A., Baijens, J. H. L. & Brouns, S. J. J. PAM-repeat associations and spacer selection preferences in single and co-occurring CRISPR-Cas systems. *Genome Biol.* **22**, 281 (2021).
40. Pyenson, N. C., Gayvert, K., Varble, A., Elemento, O. & Marraffini, L. A. Broad targeting specificity during bacterial type III CRISPR-Cas immunity constrains viral escape. *Cell Host Microbe* **22**, 343-353.e3 (2017).
41. Chabas, H., Müller, V., Bonhoeffer, S. & Regoes, R. R. Epidemiological and evolutionary consequences of different types of CRISPR-Cas systems. *PLOS Comput. Biol.* **18**, e1010329 (2022).
42. Brodt, A., Lurie-Weinberger, M. N. & Gophna, U. CRISPR loci reveal networks of gene exchange in archaea. *Biol. Direct* **6**, 65 (2011).
43. Paper, W. *et al. Ignicoccus hospitalis sp.* nov., the host of '*Nanoarchaeum equitans*'. *Int. J. Syst. Evol. Microbiol.* **57**, 803–808 (2007).
44. Dombrowski, N., Teske, A. P. & Baker, B. J. Expansive microbial metabolic versatility and biodiversity in dynamic Guaymas Basin hydrothermal sediments. *Nat. Commun.* **9**, 4999 (2018).
45. Hohenester, E. & Yurchenco, P. D. Laminins in basement membrane assembly. *Cell Adhes. Migr.* **7**, 56–63 (2013).
46. Hohenester, E. Laminin G-like domains: dystroglycan-specific lectins. *Seq. Topol. ● Carbohydr.* **56**, 56–63 (2019).

47. Benner, S. A., Ellington, A. D. & Tauer, A. Modern metabolism as a palimpsest of the RNA world. *Proc. Natl. Acad. Sci.* **86**, 7054–7058 (1989).
48. Joshi, N. A. & Fass, J. N. Sickle: A sliding-window, adaptive, quality-based trimming tool for FastQ files (Version 1.33) [Software]. (2011).
49. Nurk, S., Meleshko, D., Korobeynikov, A. & Pevzner, P. A. metaSPAdes: a new versatile metagenomic assembler. *Genome Res.* **27**, 824–834 (2017).
50. Langmead, B. & Salzberg, S. L. Fast gapped-read alignment with Bowtie 2. *Nat. Methods* **9**, 357–359 (2012).
51. Bornemann, T. L. V., Esser, S. P., Stach, T. L., Burg, T. & Probst, A. J. uBin – a manual refining tool for genomes from metagenomes. *Environ. Microbiol.* (2023).
52. Parks, D. H., Imelfort, M., Skennerton, C. T., Hugenholtz, P. & Tyson, G. W. CheckM: assessing the quality of microbial genomes recovered from isolates, single cells, and metagenomes. *Genome Res.* **25**, 1043–1055 (2015).
53. Eddy, S. R. Accelerated Profile HMM Searches. *PLOS Comput. Biol.* **7**, e1002195 (2011).
54. Darling, A. E. *et al.* PhyloSift: phylogenetic analysis of genomes and metagenomes. *PeerJ* **2**, e243 (2014).
55. Edgar, R. C. MUSCLE: multiple sequence alignment with high accuracy and high throughput. *Nucleic Acids Res.* **32**, 1792–1797 (2004).
56. Criscuolo, A. & Gribaldo, S. BMGE (Block Mapping and Gathering with Entropy): A new software for selection of phylogenetic informative regions from multiple sequence alignments. *BMC Evol. Biol.* **10**, 210 (2010).

57. Minh, B. Q. *et al.* IQ-TREE 2: New models and efficient methods for phylogenetic inference in the genomic era. *Mol. Biol. Evol.* **37**, 1530–1534 (2020).
58. Kalyaanamoorthy, S., Minh, B. Q., Wong, T. K. F., von Haeseler, A. & Jermiin, L. S. ModelFinder: fast model selection for accurate phylogenetic estimates. *Nat. Methods* **14**, 587–589 (2017).
59. Wang, H.-C., Minh, B. Q., Susko, E. & Roger, A. J. Modeling site heterogeneity with posterior mean site frequency profiles accelerates accurate phylogenomic estimation. *Syst. Biol.* **67**, 216–235 (2017).
60. Hoang, D. T., Chernomor, O., von Haeseler, A., Minh, B. Q. & Vinh, L. S. UFBoot2: Improving the ultrafast bootstrap approximation. *Mol. Biol. Evol.* **35**, 518–522 (2017).
61. Guindon, S. *et al.* New algorithms and methods to estimate maximum-likelihood phylogenies: Assessing the performance of PhyML 3.0. *Syst. Biol.* **59**, 307–321 (2010).
62. Anisimova, M., Gil, M., Dufayard, J.-F., Dessimoz, C. & Gascuel, O. Survey of branch support methods demonstrates accuracy, power, and robustness of fast likelihood-based approximation schemes. *Syst. Biol.* **60**, 685–699 (2011).
63. Letunic, I. & Bork, P. Interactive Tree Of Life (iTOL) v4: recent updates and new developments. *Nucleic Acids Res.* **47**, W256–W259 (2019).
64. Buchfink, B., Xie, C. & Huson, D. H. Fast and sensitive protein alignment using DIAMOND. *Nat. Methods* **12**, 59 (2014).
65. Gouy, M., Tannier, E., Comte, N. & Parsons, D. P. Seaview Version 5: A multiplatform software for multiple sequence alignment, molecular phylogenetic analyses, and tree

reconciliation. in *Multiple Sequence Alignment: Methods and Protocols* (ed. Katoh, K.) 241–260 (Springer US, 2021).

66. Couvin, D. *et al.* CRISPRCasFinder, an update of CRISRFinder, includes a portable version, enhanced performance and integrates search for Cas proteins. *Nucleic Acids Res* **46**, W246–W251 (2018).
67. Moller, A. G. & Liang, C. MetaCRAST: reference-guided extraction of CRISPR spacers from unassembled metagenomes. *PeerJ* **5:e3788**, e3788 (2017).
68. Fu, L., Niu, B., Zhu, Z., Wu, S. & Li, W. CD-HIT: accelerated for clustering the next-generation sequencing data. *Bioinformatics* **28**, 3150–3152 (2012).
69. Biswas, A., Fineran, P. C. & Brown, C. M. Accurate computational prediction of the transcribed strand of CRISPR non-coding RNAs. *Bioinformatics* **30**, 1805–13 (2014).
70. Roux, S., Enault, F., Hurwitz, B. L. & Sullivan, M. B. VirSorter: mining viral signal from microbial genomic data. *PeerJ* **3:e985**, e985 (2015).
71. Xie, Z. & Tang, H. ISEScan: automated identification of insertion sequence elements in prokaryotic genomes. *Bioinformatics* **33**, 3340–3347 (2017).
72. Edgar, R. C. Search and clustering orders of magnitude faster than BLAST. *Bioinformatics* **26**, 2460–2461 (2010).
73. Altschul, S. F., Gish, W., Miller, W., Myers, E. W. & Lipman, D. J. Basic local alignment search tool. *J. Mol. Biol.* **215**, 403–410 (1990).
74. Nayfach, S. *et al.* CheckV assesses the quality and completeness of metagenome-assembled viral genomes. *Nat. Biotechnol.* **39**, 578–585 (2021).

75. Cook, R. *et al.* INfrastructure for a PHAge REference Database: Identification of large-scale biases in the current collection of cultured phage genomes. *PHAGE* **2**, 214–223 (2021).
76. Bolduc, B. *et al.* vConTACT: an iVirus tool to classify double-stranded DNA viruses that infect Archaea and Bacteria. *PeerJ* **5**, e3243 (2017).
77. Bin Jang, H. *et al.* Taxonomic assignment of uncultivated prokaryotic virus genomes is enabled by gene-sharing networks. *Nat. Biotechnol.* **37**, 632–639 (2019).
78. Meier-Kolthoff, J. P. & Göker, M. VICTOR: genome-based phylogeny and classification of prokaryotic viruses. *Bioinformatics* **33**, 3396–3404 (2017).
79. Moraru, C., Varsani, A. & Kropinski, A. M. VIRIDIC—A novel tool to calculate the intergenomic similarities of prokaryote-infecting Viruses. *Viruses* **12**, (2020).
80. Meier-Kolthoff, J. P., Auch, A. F., Klenk, H.-P. & Göker, M. Genome sequence-based species delimitation with confidence intervals and improved distance functions. *BMC Bioinformatics* **14**, 60 (2013).
81. Lefort, V., Desper, R. & Gascuel, O. FastME 2.0: A comprehensive, accurate, and fast distance-based phylogeny inference program. *Mol. Biol. Evol.* **32**, 2798–2800 (2015).
82. Farris, J. S. Estimating phylogenetic trees from distance matrices. *Am. Nat.* **106**, 645–668 (1972).
83. Shannon, P. *et al.* Cytoscape: A software environment for integrated models of biomolecular interaction networks. *Genome Res.* **13**, 2498–2504 (2003).
84. Nishimura, Y. *et al.* ViPTree: the viral proteomic tree server. *Bioinformatics* **33**, 2379–2380 (2017).

85. Li, H. *et al.* The sequence alignment/map format and SAMtools. *Bioinformatics* **25**, 2078–2079 (2009).
86. Quinlan, A. R. & Hall, I. M. BEDTools: a flexible suite of utilities for comparing genomic features. *Bioinformatics* **26**, 841–842 (2010).
87. Team, R. C. *R: A language and environment for statistical computing*. (Vienna, Austria, 2013).
88. Zhang, Y. & Sievert, S. Pan-genome analyses identify lineage- and niche-specific markers of evolution and adaptation in *Epsilonproteobacteria*. *Front. Microbiol.* **5**, 110 (2014).
89. Dufault-Thompson, K., Steffensen, J. L. & Zhang, Y. Using PSAMM for the curation and analysis of genome-scale metabolic models. in *Metabolic Network Reconstruction and Modeling: Methods and Protocols* (ed. Fondi, M.) 131–150 (Springer New York, 2018).
90. Steffensen, J. L., Dufault-Thompson, K. & Zhang, Y. PSAMM: A portable system for the analysis of metabolic models. *PLoS Comput. Biol.* **12**, e1004732–e1004732 (2016).
91. Li, W. & Godzik, A. Cd-hit: a fast program for clustering and comparing large sets of protein or nucleotide sequences. *Bioinformatics* **22**, 1658–1659 (2006).
92. Gonnerman, M. C., Benedict, M. N., Feist, A. M., Metcalf, W. W. & Price, N. D. Genomically and biochemically accurate metabolic reconstruction of *Methanosarcina barkeri* Fusaro, iMG746. *Biotechnol. J.* **8**, 1070–1079 (2013).
93. Goyal, N., Widiastuti, H., Karimi, I. A. & Zhou, Z. A genome-scale metabolic model of *Methanococcus maripaludis* S_2 for CO_2 capture and conversion to methane. *Mol. Biosyst.* **10**, 1043–1054 (2014).

94. Kanehisa, M., Furumichi, M., Tanabe, M., Sato, Y. & Morishima, K. KEGG: new perspectives on genomes, pathways, diseases and drugs. *Nucleic Acids Res.* **45**, D353–D361 (2017).

95. Huerta-Cepas, J. *et al.* eggNOG 5.0: a hierarchical, functionally and phylogenetically annotated orthology resource based on 5090 organisms and 2502 viruses. *Nucleic Acids Res.* **47**, D309–D314 (2019).

96. Saier, M. H., Jr *et al.* The transporter classification database (TCDB): recent advances. *Nucleic Acids Res.* **44**, D372–D379 (2016).

97. Neidhardt, F. C., Neidhardt, F. C. N., Ingraham, J. L. & Schaechter, M. Physiology of the bacterial cell: A molecular approach. (Sinauer Associates, 1990).

98. Nelson, D. L., Nelson, R. D. & Cox, M. M. *Lehninger Principles of Biochemistry, Fourth Edition + Lecture Notebook*. (W.H. Freeman, 2004).

99. Biswas, A., Gagnon, J. N., Brouns, S. J. J., Fineran, P. C. & Brown, C. M. CRISPRTarget: bioinformatic prediction and analysis of crRNA targets. *RNA Biol.* **10**, 817–827 (2013).

100. Crooks, G. E., Hon, G., Chandonia, J.-M. & Brenner, S. E. WebLogo: A sequence logo generator. *Genome Res.* **14**, 1188–1190 (2004).

101. Schneider, T. D. & Stephens, R. M. Sequence logos: a new way to display consensus sequences. *Nucleic Acids Res.* **18**, 6097–6100 (1990).

102. Koboldt, D. C. *et al.* VarScan 2: Somatic mutation and copy number alteration discovery in cancer by exome sequencing. *Genome Res.* **22**, 568–576 (2012).

103. Oberortner, E., Cheng, J.-F., Hillson, N. J. & Deutsch, S. Streamlining the design-to-build transition with build-optimization software tools. *ACS Synth. Biol.* **6**, 485–496 (2017).

104. Garamella, J., Marshall, R., Rustad, M. & Noireaux, V. The All E. coli TX-TL Toolbox 2.0: A Platform for Cell-Free Synthetic Biology. *ACS Synth. Biol.* **5**, 344–355 (2016).

105. Shin, J. & Noireaux, V. An *E. coli* cell-free expression toolbox: Application to synthetic gene circuits and artificial cells. *ACS Synth. Biol.* **1**, 29–41 (2012).

106. Leenay, R. T. *et al.* Identifying and visualizing functional PAM diversity across CRISPR-Cas systems. *Mol. Cell* **62**, 137–147 (2016).

107. Ondov, B. D., Bergman, N. H. & Phillippy, A. M. Interactive metagenomic visualization in a Web browser. *BMC Bioinformatics* **12**, 385 (2011).

108. Chaumeil, P.-A., Mussig, A. J., Hugenholtz, P. & Parks, D. H. GTDB-Tk: a toolkit to classify genomes with the Genome Taxonomy Database. *Bioinformatics* **36**, 1925–1927 (2020).

109. Parks, D. H. *et al.* A standardized bacterial taxonomy based on genome phylogeny substantially revises the tree of life. *Nat. Biotechnol.* **36**, 996–1004 (2018).

110. Parks, D. H. *et al.* A complete domain-to-species taxonomy for Bacteria and Archaea. *Nat. Biotechnol.* **38**, 1079–1086 (2020).

111. Chen, I.-M. A. *et al.* IMG/M v.5.0: an integrated data management and comparative analysis system for microbial genomes and microbiomes. *Nucleic Acids Res.* **47**, D666–D677 (2019).

112. Sharrar, A. M. *et al.* Novel large sulfur bacteria in the metagenomes of groundwater-fed chemosynthetic microbial mats in the Lake Huron Basin. *Front. Microbiol.* **8**, 791 (2017).

113. Bird, J. T., Baker, B. J., Probst, A. J., Podar, M. & Lloyd, K. G. Culture independent genomic comparisons reveal environmental adaptations for Altiarchaeales. *Front. Microbiol.* **7**, (2016).

114. Posit team. Rstudio: Integrated development environment for R. (2022).

115. Esser, S. P. & Probst, A. J. Genomes of Ca. Altiarchaeum and Ca. Huberiarchaeum from Crystal Geyser and Horonobe Underground Research Laboratory. (2023) doi:10.6084/m9.figshare.22339555.

116. Esser, S. P., Rahlff, J. & Probst, A. J. Viral operational taxonomic units (vOTUs) derived from metagenomes from Crystal Geyser. (2023) doi:10.6084/m9.figshare.22738568.

117. Turzynski, V., Esser, S. P. & Probst, A. J. FISH images of *Ca.* Altiarchaeum and *Ca.* Huberiarchaeum in Crystal Geyser and Horonobe Underground Research Laboratory. (2023) doi:10.6084/m9.figshare.22739849.

Figure 1. Phylogenetic positioning of Ca. Altiarchaea and Ca. Huberarchaea, sampling locations, FISH analysis, and CRISPR-Cas targets | (A) *Phylogenetic tree of archaea highlighting Candidatus Altiarchaeum and Candidatus Huberiarchaeum of the sampling locations Crystal Geyser (CG, Utah, USA, orange) and Horonobe Underground Research Laboratory (HURL, Hokkaido, Japan, green). Fluorescence pictures show Ca. Altiarchaeum (blue; H - host) as host and its episymbiont Ca. Huberiarchaeum (orange; S - symbiont) in the respective ecosystems. Scale bar 1 µm.* ***(B)*** *Ca. Altiarchaea CRISPR systems, their associated conserved direct repeat (DR) sequences (with exception of a point mutation marked in red), and the number of spacer clusters (97% nucleotide identity) arising from the two sampling sites.* ***(C)*** *Logarithmic number of centroid spacers derived from spacer clusters matching 64 extracted viral sequences (total number of spacer matches: 0 of unassigned CRISPR system and 16561 of CRISPR system IB), 17 binned genomes of Ca. Altiarchaeum crystalense (total number of spacer matches: 115 of unassigned CRISPR system and 1,311 of CRISPR system IB) and 11 binned genomes of Ca. Huberiarchaeum crystalense (total number of spacer matches: 0 of unassigned CRISPR system and 1,445 of CRISPR system IB) originating from the CG site (Table S2). Spacers were derived from the complete 66-sample metagenomic dataset.* ***(D)*** *Percentage of CRISPR system I-B spacer cluster abundances matching to organisms that were previously detected in this ecosystem at the CG site. Listed are the logarithmic genome abundances of the respective organisms. Error bars denote the standard deviation of the abundance of matching spacer clusters for samples CG05, CG08, and CG16 of the year 2015. These were displayed because also transcriptomic data was available. The dataset of HURL is referring to one metagenome, as no other data was available. (Means and standard deviation: CG Altiarchaeum crystalense: 2.69 $\pm$ 0.21, 1.93 $\pm$ 0.24; Huberiarchaeum crystalense: 2.99 $\pm$0.23, 2.19 $\pm$0.23; HURL Altiarchaeum horonobense: 0.029; Huberiarchaeum julieae: 0.019)* ***(E)*** *Logarithmic number of centroid spacers derived from spacer clusters matching extracted viral sequences (total number of spacer matches: 64 of unassigned CRISPR system and 22 of CRISPR system IB), two binned genomes of Ca. Altiarchaeum horonobense (total number of spacer matches: 19 of unassigned CRISPR system and 2 of CRISPR system IB) and one binned genome of Ca. Huberiarchaeum julieae (total number of spacer matches: 7 of unassigned CRISPR system and*

0 of CRISPR system IB) originating from the HURL site. Spacers were derived from one metagenomic dataset.

Figure 2. Example of Ca. Altiarchaea CRISPR-Cas type IB loci, gene targets on host and episymbiont genomes, and metabolic interactions between Ca. Altiarchaea and Ca. Huberiarchaea as inferred from genome-scaled metabolic modeling | (A) Example of *CRISPR system I-B locus of Ca. A. crystalense with assembled CRISPR array from a single amplified genome (accession no. 1088571). Red box highlights the analysed CRISPR array bearing the repeat sequence GTTTAAATCGTACTATGTAGTATGGAAAC and its respective spacers within the array.* ***(B)*** *Example of a Ca. A. crystalense DNA polymerase II large subunit locus self-targeted by altiarchaeal spacers extracted from metagenomes (accession no. 2786546692). Red boxes on the genomic region highlight spacer matching regions. Yellow genes are annotated as uncharacterized proteins.* ***(C)*** *Example of a Ca. H. crystalense genome (accession no. 2785510793) partially matched by Ca. A. crystalense spacers at the genetic loci of the 30S ribosomal protein S11, CTP synthase, and an uncharacterized protein.* ***(D)*** *Example of a Ca. H. crystalense SAG (accession no. 1088571) partially matched by Ca. A. crystalense spacers at the genetic loci of uncharcterized proteins.* ***(E)*** *Metabolic interactions between Ca. Altiarchaeum and Ca. Huberiarchaeum in Crystal Geyser, CG (17 genomes of Ca. A. crystalense and eleven of Ca. H. crystalense, and spacers extracted from transcriptomes) and in* ***(F)*** *Horonobe Underground Research Laboratory, HURL (one genome of A. horonobense and one Ca. H. julieae). Solid arrows denote exchanges of putative essential metabolites between Ca. Altiarchaeum and Ca. Huberiarchaeum. Dashed arrows indicate exchange of metabolites that are only required when CRISPR spacers attack certain target genes (type I-B labeled with red diamonds and the unassigned type labeled with green diamonds).* ***(E-F)*** *While most compounds were produced by Ca. Altiarchaea, the production of dUMP requires an essential gene, ⑤-dCMP deaminase (EC 3.5.4.12), in Huberiarchaea. Circled numbers indicate key enzymes involved in symbiotic metabolic interactions at CG: ①–Phenylalanyl-tRNA synthetase (EC 6.1.1.20), Lysyl-tRNA synthetase (EC 6.1.1.6); ②, ③–(d)NDP kinase (EC 2.7.4.6); ④–dCMP kinase (EC 2.7.4.25); ⑤–dCMP deaminase (EC 3.5.4.12); ⑥, ⑦–dTMP synthase (EC 2.1.1.45); ⑧–FAD-dependent dTMP*

synthase (EC 2.1.1.148). The production of tetrahydrofolate (THF) requires an essential gene encoded by Ca. Huberiarchaeum julieae, ⑬–dTMP synthase (EC 2.1.1.45). Circled numbers denote key enzymes involved in the symbiotic metabolic interactions at HURL: ⑬–dTMP synthase (EC 2.1.1.45); ⑫–FAD-dependent dTMP synthase (EC 2.1.1.148); ⑨, ⑩–dCTP deaminase (EC 3.5.4.13); ⑪–dUTPase (EC 3.6.1.23); and ⑭–Dihydrofolate synthase (EC 6.3.2.12).

Figure 3. Illustration of the newly discovered functionality of CRISPR-Cas systems within Ca. Altiarchaea | ***a. Viral targeting:*** *CRISPR-Cas system targets the genomes of MGEs that infect the cell (current state of knowledge).* ***b. Targeting of episymbiont:*** *CRISPR-Cas system targets the genome of the episymbiont Ca. Huberiarchaeum to defend against the parasite.* ***c. Self-targeting and respective metabolic complementation:*** *Self-targeting of CRISPR-Cas in Altiarchaea mediates metabolic patchiness, which is complemented by the episymbiont metabolism, leading to mutualism. Please note, that this mutualism might be limited to a subset of organisms in the host population. Arrows symbolize spacer-protospacer interactions. The Figure was created with Biorender.com.*

Figure 4. Directed spacer interaction of DPANN archaea derived from the analysis of 7,012 publicly available archaeal genomes | *Nodes correspond to archaeal genomes. Boomerang and linear grey arrows indicate self-targeting and non-self (including interspecies) targeting spacers, respectively. With the exception of Thermoprotei and Bathyarchaeota, all of the archaea pictured belong to the DPANN superphylum. Colors represent the phylogenetic affiliation of genomes. Genomes of Ca. Altiarchaeum and Ca. Huberiarchaeum derives primarily from CG. Genomes coded according to their corresponding ecosystem: CG - Crystal Geyser[20,25,27]; LHB - Lake Huron Basin[112]; WOR - White Oak River[113]; GUAY - Guaymas Basin[44]; HURL - Horonobe Underground Research Laboratory[24].*

Extended Data Fig. 1 | Correlation of repeat abundance and abundance of Ca. Altiarchaea genomes. *Spearman rank correlation (two-tailed) of logarithmic abundances of Ca. A. crystalense and logarithmic abundances of repeat sequences of the unassigned CRISPR array (p-value 3.4 e^{-16}) and the I-B CRISPR system ($p < 2.2\ e^{-16}$) in metagenomes from CG (n=66). The grey area depicts the confidence interval of 0.95. The line indicates that the correlation of the genome abundance and repeat abundance is linear. Visualization was performed with R[87,114] (version 3.6.1).*

Extended Data Fig. 2 | Viral clusters predicted by VIRIDIC[79]. *Heatmap showing intergenomic similarity for viral scaffolds of viral clusters (VC_XY) and some singletons (black). Coloring of viral OTUs (vOTUs) according to Table S6. VC_09, _12, _13 determined by the other tools were not*

found by VIRIDIC. Only scaffolds with intergenomic similarity of >10 between two viral scaffolds are shown.

Extended Data Fig. 3 | Coverage analyses of scaffolds targeted by spacers from Ca. Altiarchaea. *Coverage changes within targeted regions by CRISPR system IB of Ca. Altiarchaeum and Ca. Huberiarchaeum based on metagenomic read mapping. The vertically grey marked regions are spacer targeted regions of either Ca. Altiarchaeum or Ca. Huberiarchaeum, whereby the horizontally dark grey lines are showing the average coverage of the scaffold. The colored graphs show the coverage across the spacer targeted region of three samples from the minor eruption phase, where Ca. Altiarchaeum is the most abundant organism (Fig. S1).*

Extended Data Fig. 4 | Spacer targeting analyses of publicly available archaeal genomes. *Directed spacer analysis of 7,012 publicly available archaeal genomes (Table S4) shows large clusters of spacers targeting at species level. The targeting spacers (edges) of the genomes Sulfolobus, Methanomicrobia and Halobacterium (nodes) form large clusters performing self-targeting or targeting other genomes of the same family. The clustering was illustrated with Cytoscape[83] (version 3.9.1). Please note that targeting within the same genus might limit the interspecies recombination, as demonstrated in haloarchaea[37], or reflect the presence of multiple conserved genomic regions between the genomes.*

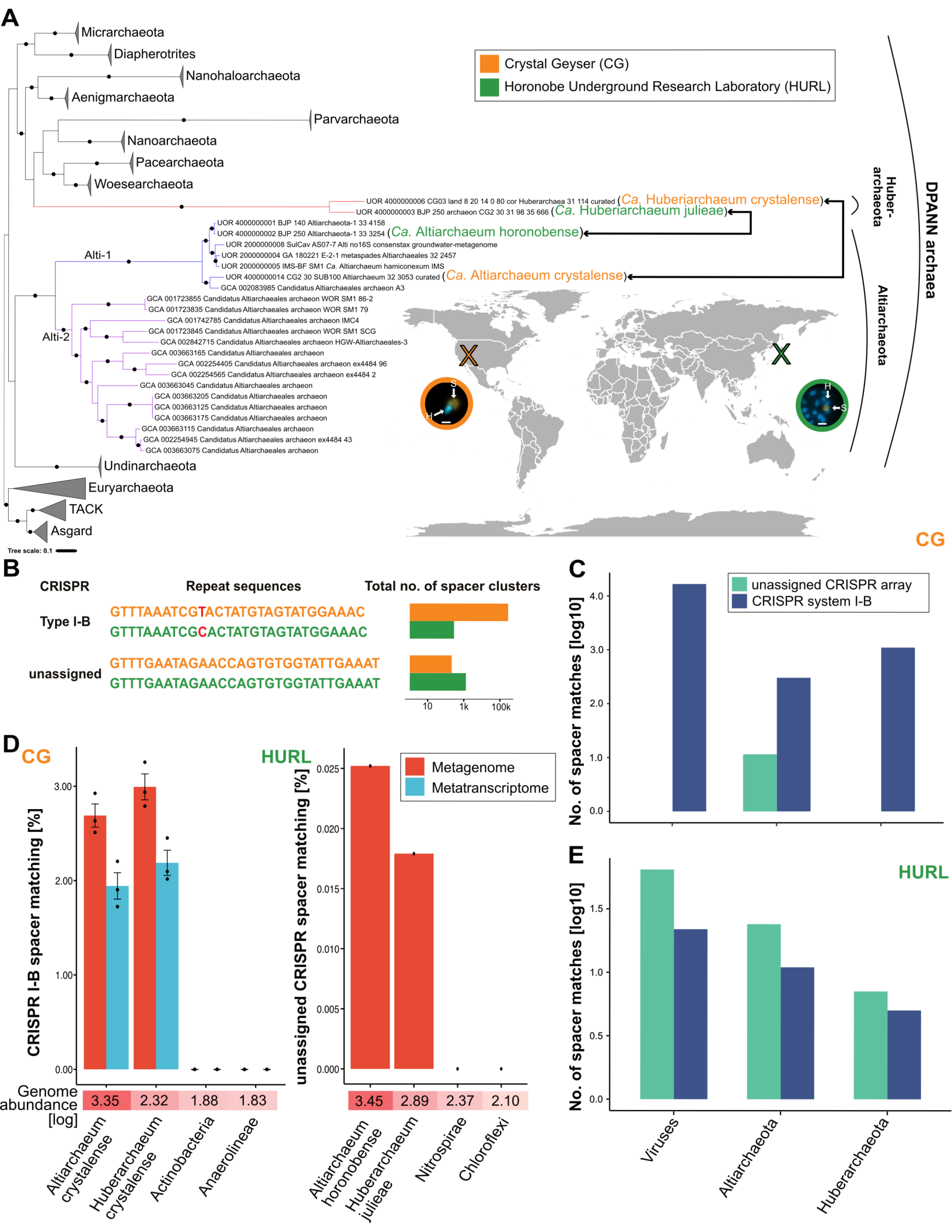
A
Crystal Geyser (CG)
Horonobe Underground Research Laboratory (HURL)
Micrarchaeota
Diapherotrites
Nanohaloarchaeota
Aenigmarchaeota
Parvarchaeota
Nanoarchaeota
Pacearchaeota
Woesearchaeota
Undinarchaeota
Euryarchaeota
TACK
Asgard
Tree scale: 0.1
Alti-1
Alti-2
UOR 4000000006 CG03 land 8 20 14 0 80 cor Huberarchaea 31 114 curated (Ca. Huberiarchaeum crystalense)
UOR 4000000003 BJP 250 archaeon CG2 30 31 98 35 666 (Ca. Huberiarchaeum julieae)
UOR 4000000001 BJP 140 Altiarchaeota-1 33 4158
UOR 4000000002 BJP 250 Altiarchaeota-1 33 3254 (Ca. Altiarchaeum horonobense)
UOR 2000000008 SulCav AS07-7 Alti no16S consenstax groundwater-metagenome
UOR 2000000004 GA 180221 E-2-1 metaspades Altiarchaeales 32 2457
UOR 2000000005 IMS-BF SM1 Ca. Altiarchaeum hamiconexum IMS
UOR 4000000014 CG2 30 SUB100 Altiarchaeum 32 3053 curated (Ca. Altiarchaeum crystalense)
GCA 002083985 Candidatus Altiarchaeales archaeon A3
GCA 001723855 Candidatus Altiarchaeales archaeon WOR SM1 86-2
GCA 001723835 Candidatus Altiarchaeales archaeon WOR SM1 79
GCA 001742785 Candidatus Altiarchaeales archaeon IMC4
GCA 001723845 Candidatus Altiarchaeales archaeon WOR SM1 SCG
GCA 002842715 Candidatus Altiarchaeales archaeon HGW-Altiarchaeales-3
GCA 003663165 Candidatus Altiarchaeales archaeon
GCA 002254405 Candidatus Altiarchaeales archaeon ex4484 96
GCA 002254565 Candidatus Altiarchaeales archaeon ex4484 2
GCA 003663045 Candidatus Altiarchaeales archaeon
GCA 003663205 Candidatus Altiarchaeales archaeon
GCA 003663125 Candidatus Altiarchaeales archaeon
GCA 003663175 Candidatus Altiarchaeales archaeon
GCA 003663115 Candidatus Altiarchaeales archaeon
GCA 002254945 Candidatus Altiarchaeales archaeon ex4484 43
GCA 003663075 Candidatus Altiarchaeales archaeon
Huber-archaeota
Altiarchaeota
DPANN archaea
CG
B
CRISPR
Repeat sequences
Total no. of spacer clusters
Type I-B
GTTTAAATCGTACTATGTAGTATGGAAAC
GTTTAAATCGCACTATGTAGTATGGAAAC
unassigned
GTTTGAATAGAACCAGTGTGGTATTGAAAT
GTTTGAATAGAACCAGTGTGGTATTGAAAT
10
1k
100k
C
unassigned CRISPR array
CRISPR system I-B
No. of spacer matches [log10]
4.0
3.0
2.0
1.0
0.0
D
CG
HURL
Metagenome
Metatranscriptome
CRISPR I-B spacer matching [%]
3.00
2.00
1.00
0.00
unassigned CRISPR spacer matching [%]
0.025
0.020
0.015
0.010
0.005
0.000
Genome abundance [log]
3.35
2.32
1.88
1.83
3.45
2.89
2.37
2.10
Altiarchaeum crystalense
Huberarchaeum crystalense
Actinobacteria
Anaerolineae
Altiarchaeum horonobense
Huberarchaeum julieae
Nitrospirae
Chloroflexi
E
HURL
No. of spacer matches [log10]
1.5
1.0
0.5
0.0
Viruses
Altiarchaeota
Huberarchaeota

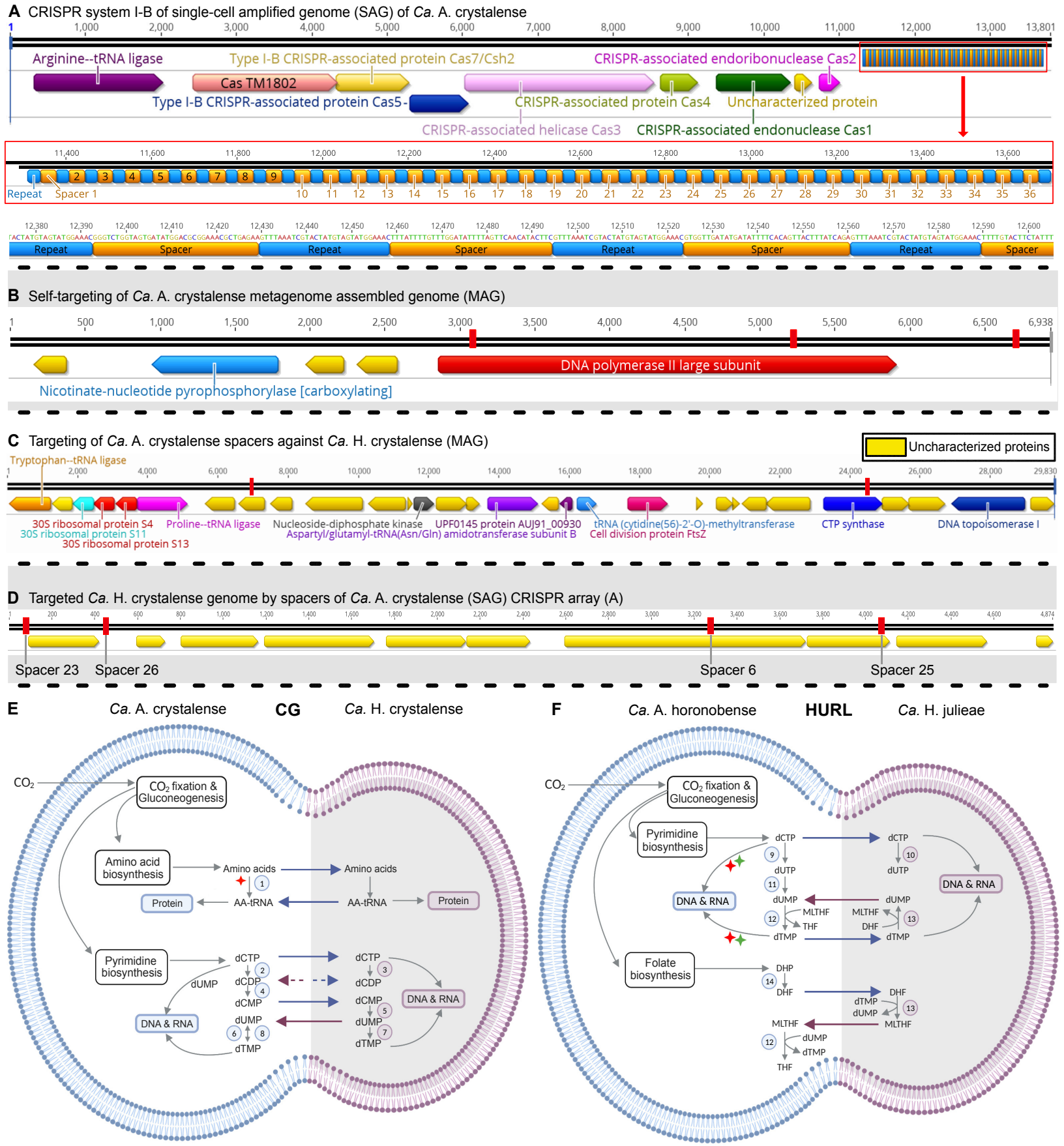
A CRISPR system I-B of single-cell amplified genome (SAG) of Ca. A. crystalense
Arginine--tRNA ligase
Type I-B CRISPR-associated protein Cas7/Csh2
CRISPR-associated endoribonuclease Cas2
Cas TM1802
Type I-B CRISPR-associated protein Cas5-
CRISPR-associated protein Cas4
Uncharacterized protein
CRISPR-associated helicase Cas3
CRISPR-associated endonuclease Cas1
Repeat
Spacer 1
Repeat
Spacer
B Self-targeting of Ca. A. crystalense metagenome assembled genome (MAG)
DNA polymerase II large subunit
Nicotinate-nucleotide pyrophosphorylase [carboxylating]
C Targeting of Ca. A. crystalense spacers against Ca. H. crystalense (MAG)
Uncharacterized proteins
Tryptophan--tRNA ligase
30S ribosomal protein S4
30S ribosomal protein S11
30S ribosomal protein S13
Proline--tRNA ligase
Nucleoside-diphosphate kinase
Aspartyl/glutamyl-tRNA(Asn/Gln) amidotransferase subunit B
UPF0145 protein AUJ91_00930
tRNA (cytidine(56)-2'-O)-methyltransferase
Cell division protein FtsZ
CTP synthase
DNA topoisomerase I
D Targeted Ca. H. crystalense genome by spacers of Ca. A. crystalense (SAG) CRISPR array (A)
Spacer 23
Spacer 26
Spacer 6
Spacer 25
E
Ca. A. crystalense
CG
Ca. H. crystalense
F
Ca. A. horonobense
HURL
Ca. H. julieae
CO2
CO2 fixation & Gluconeogenesis
Amino acid biosynthesis
Amino acids
AA-tRNA
Protein
Pyrimidine biosynthesis
dCTP
dCDP
dCMP
dUMP
dTMP
DNA & RNA
Folate biosynthesis
DHP
DHF
THF
MLTHF
dUTP

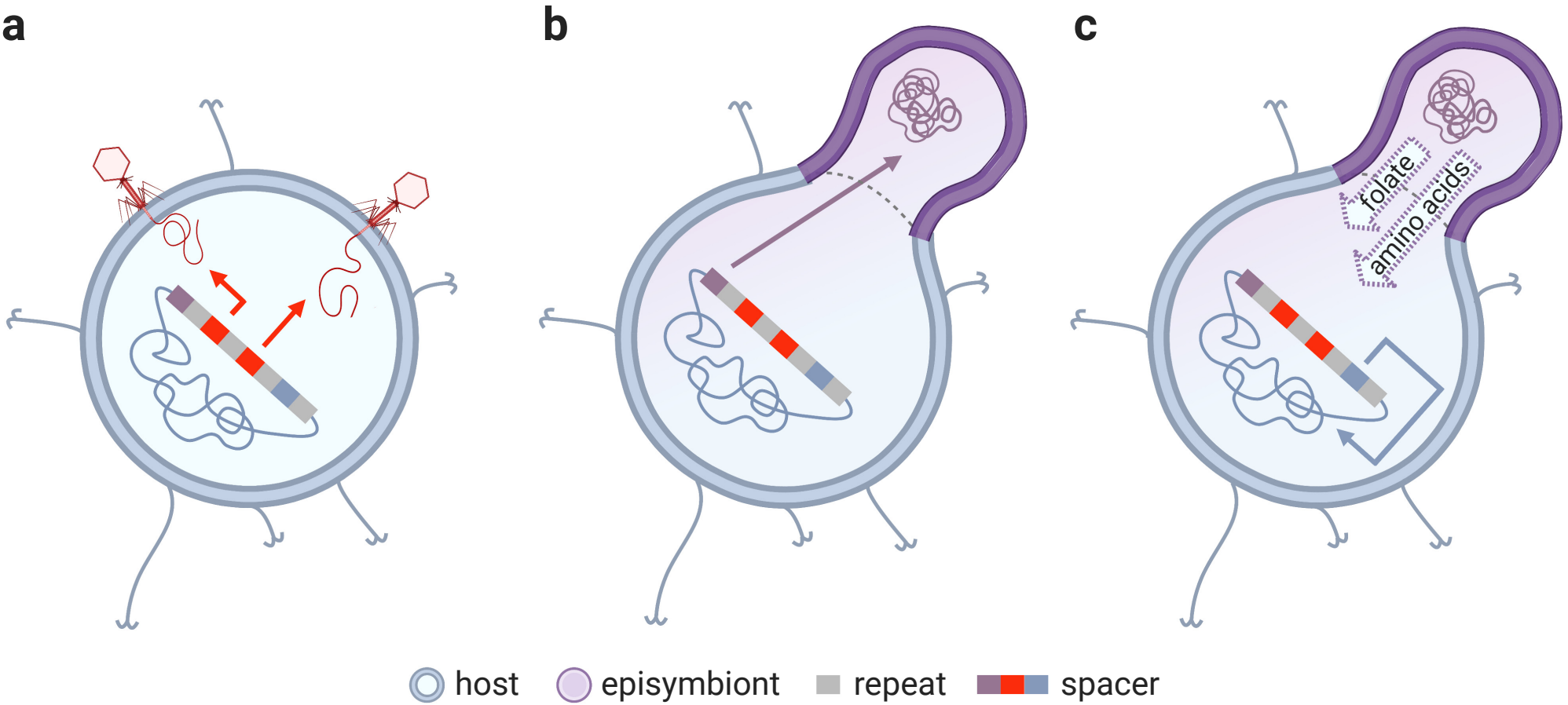

a) Viral targeting. **b)** Targeting of episymbiont. **c)** Self-targeting and respective metabolic complementation.

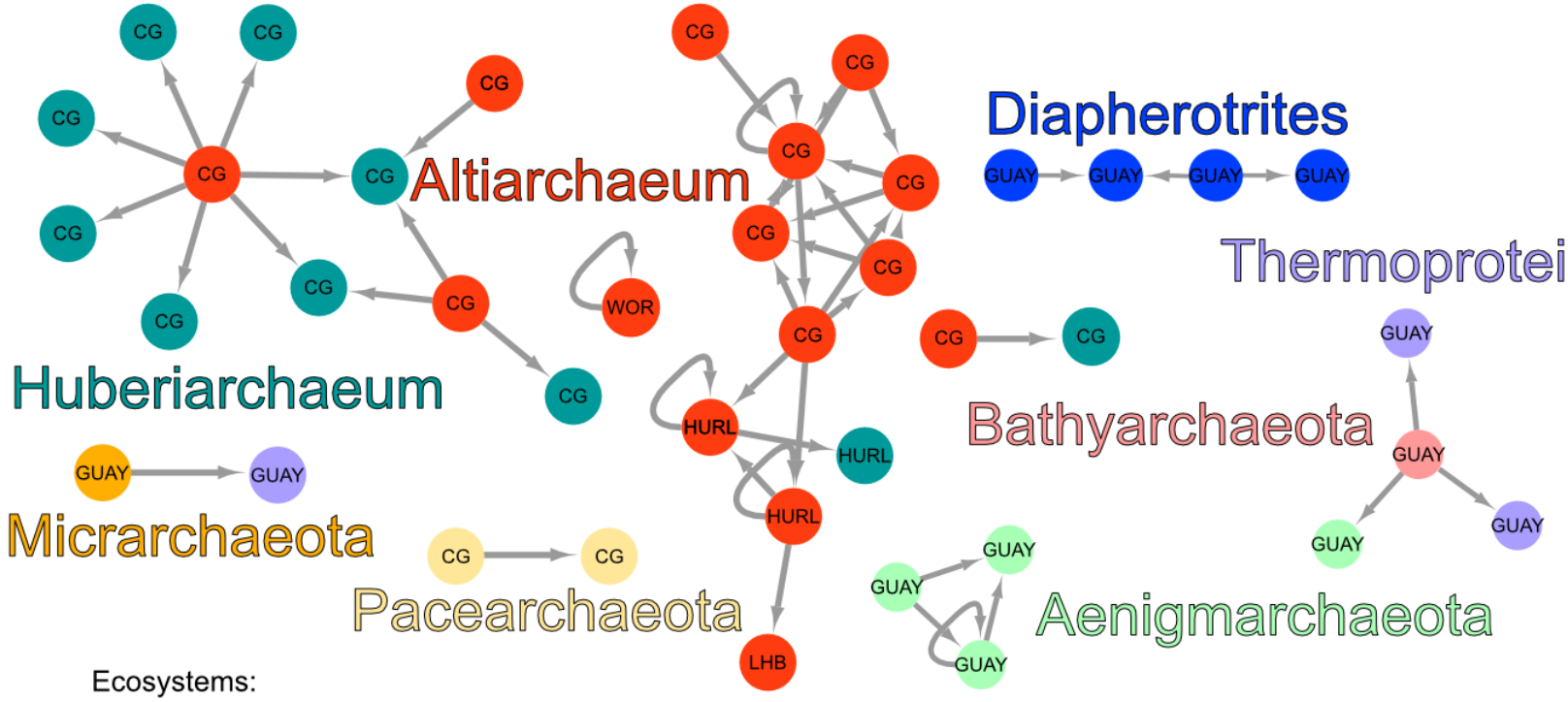

Ecosystems:
CG - Crystal Geyser
HURL - Horonobe Underground R. Lab.
GUAY - Guaymas Basin
LHB - Lake Huron Basin
WOR - White Oak River

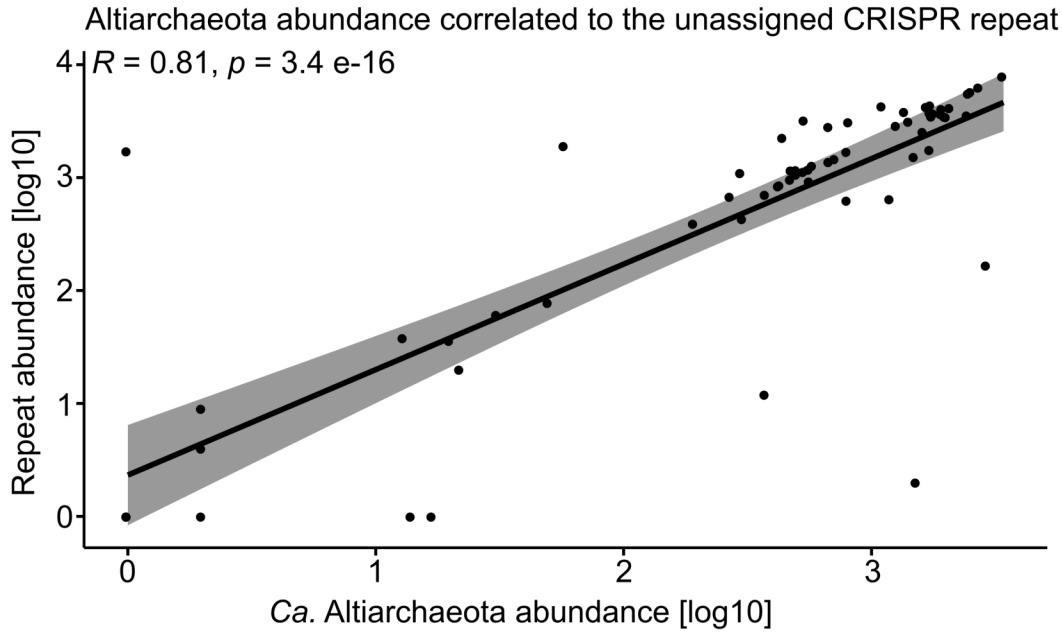
Altiarchaeota abundance correlated to the unassigned CRISPR repeat
R = 0.81, p = 3.4 e-16
Repeat abundance [log10]
Ca. Altiarchaeota abundance [log10]
0
1
2
3
4

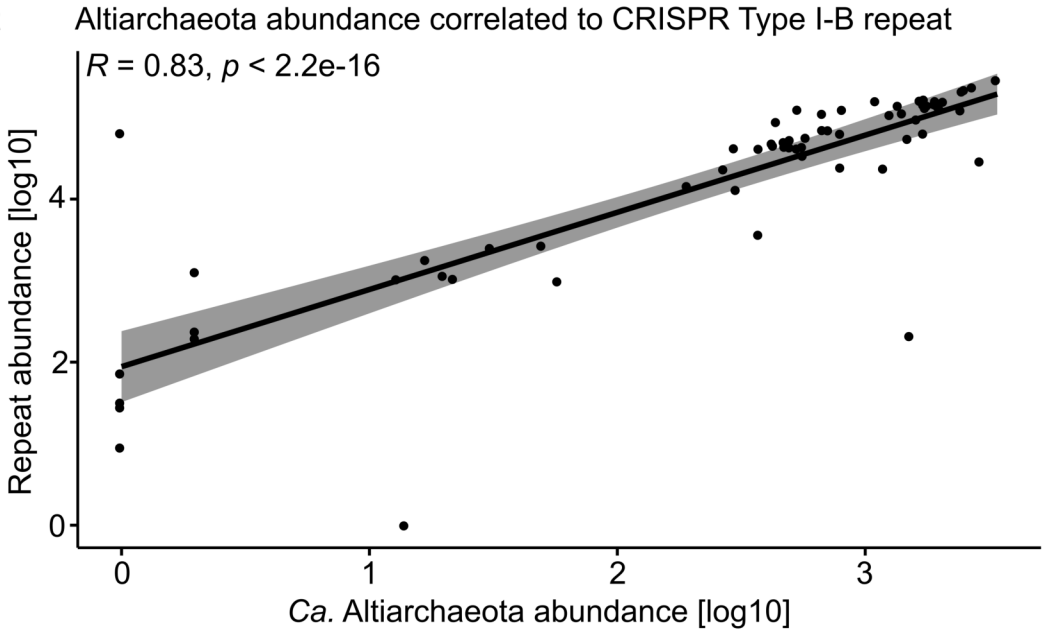
Altiarchaeota abundance correlated to CRISPR Type I-B repeat
R = 0.83, p < 2.2e-16
Repeat abundance [log10]
Ca. Altiarchaeota abundance [log10]
0
1
2
3
4

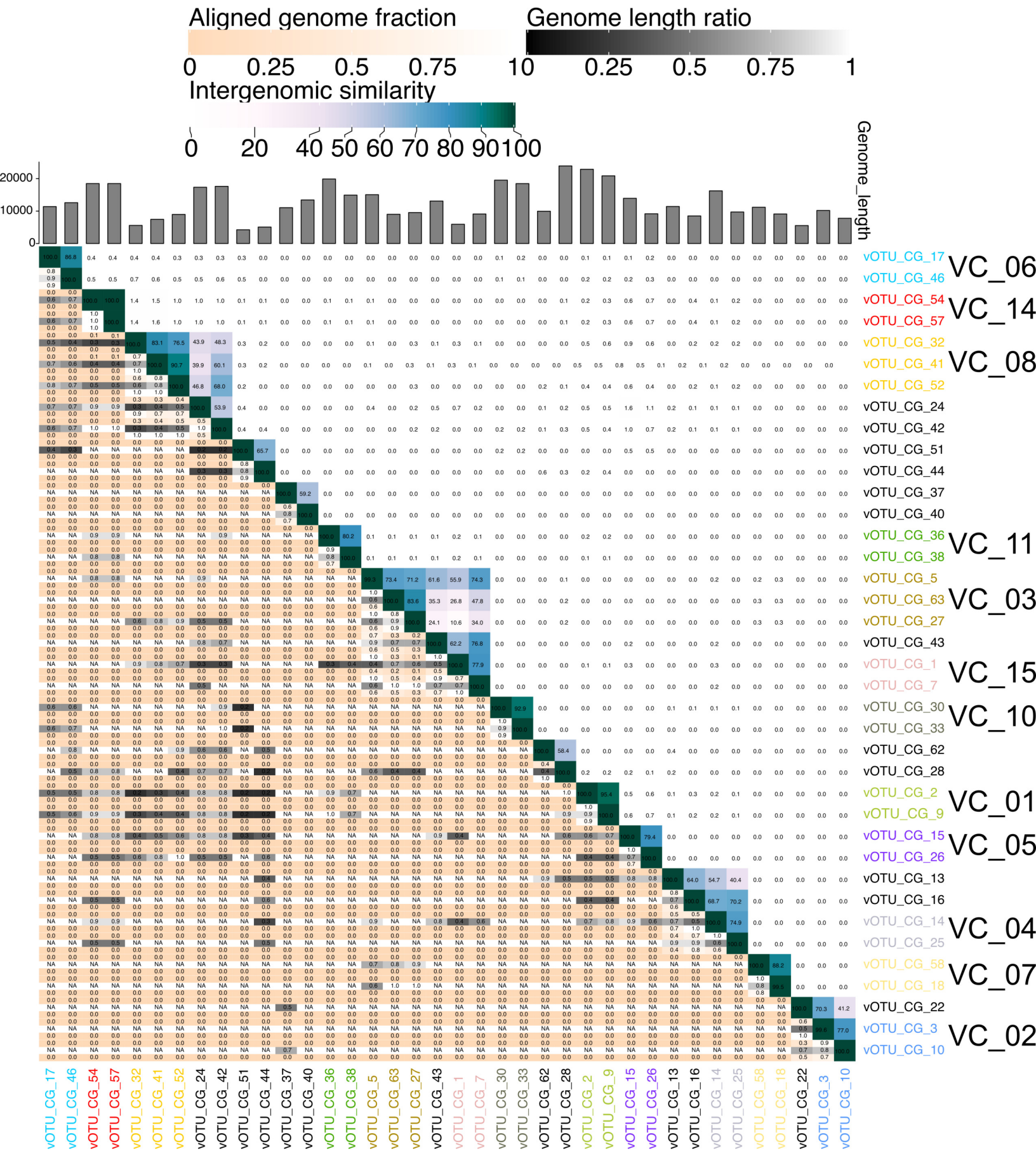
Aligned genome fraction
0
0.25
0.5
0.75
1
Genome length ratio
0
0.25
0.5
0.75
1
Intergenomic similarity
0
20
40
50
60
70
80
90
100
Genome_length
20000
10000
0
vOTU_CG_17
vOTU_CG_46
vOTU_CG_54
vOTU_CG_57
vOTU_CG_32
vOTU_CG_41
vOTU_CG_52
vOTU_CG_24
vOTU_CG_42
vOTU_CG_51
vOTU_CG_44
vOTU_CG_37
vOTU_CG_40
vOTU_CG_36
vOTU_CG_38
vOTU_CG_5
vOTU_CG_63
vOTU_CG_27
vOTU_CG_43
vOTU_CG_1
vOTU_CG_7
vOTU_CG_30
vOTU_CG_33
vOTU_CG_62
vOTU_CG_28
vOTU_CG_2
vOTU_CG_9
vOTU_CG_15
vOTU_CG_26
vOTU_CG_13
vOTU_CG_16
vOTU_CG_14
vOTU_CG_25
vOTU_CG_58
vOTU_CG_18
vOTU_CG_22
vOTU_CG_3
vOTU_CG_10
VC_06
VC_14
VC_08
VC_11
VC_03
VC_15
VC_10
VC_01
VC_05
VC_04
VC_07
VC_02

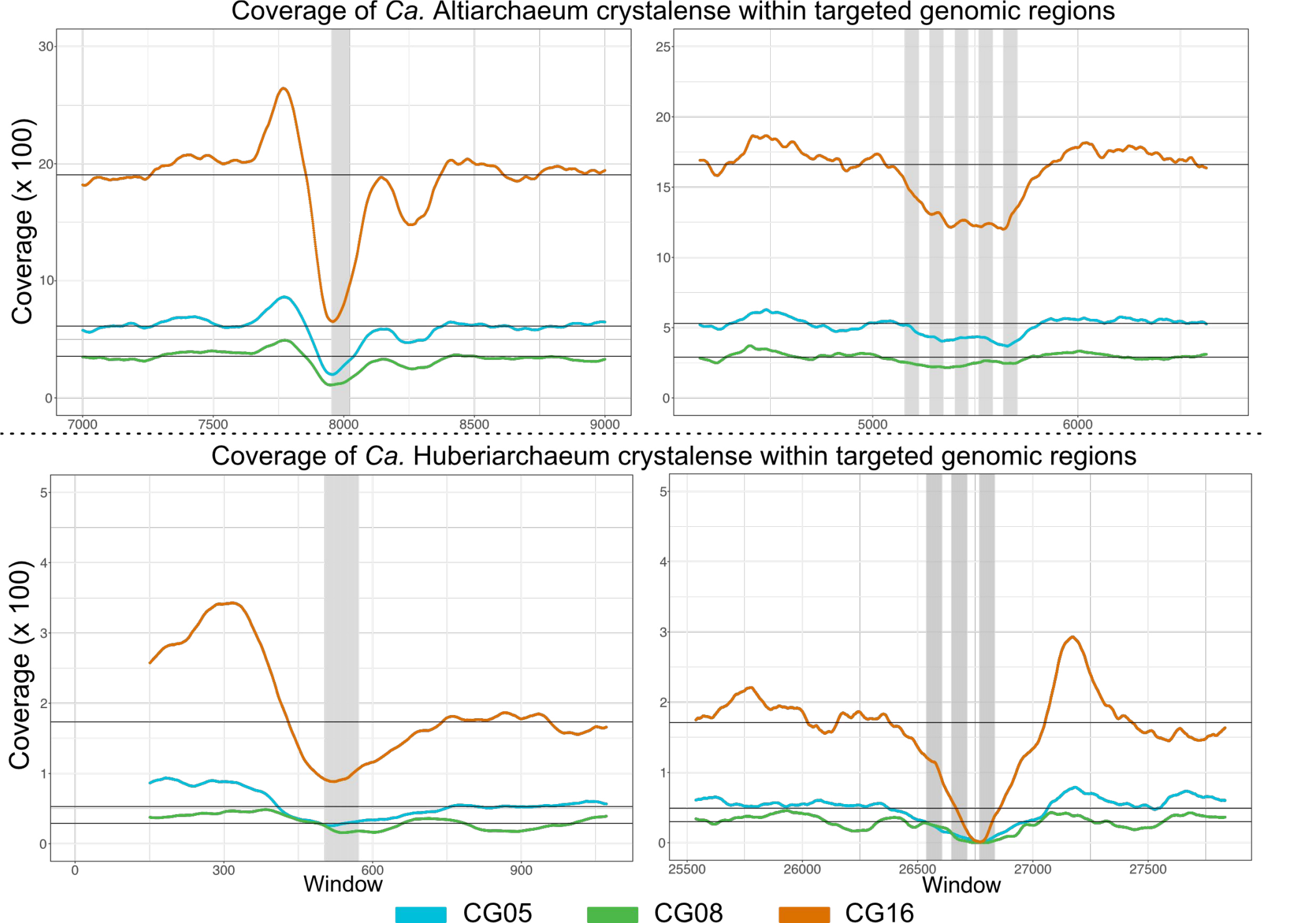
Coverage of Ca. Altiarchaeum crystalense within targeted genomic regions
Coverage (x 100)
30
20
10
0
7000
7500
8000
8500
9000
25
20
15
10
5
0
5000
6000
Coverage of Ca. Huberiarchaeum crystalense within targeted genomic regions
Coverage (x 100)
5
4
3
2
1
0
0
300
600
900
Window
25500
26000
26500
27000
27500
Window
CG05
CG08
CG16

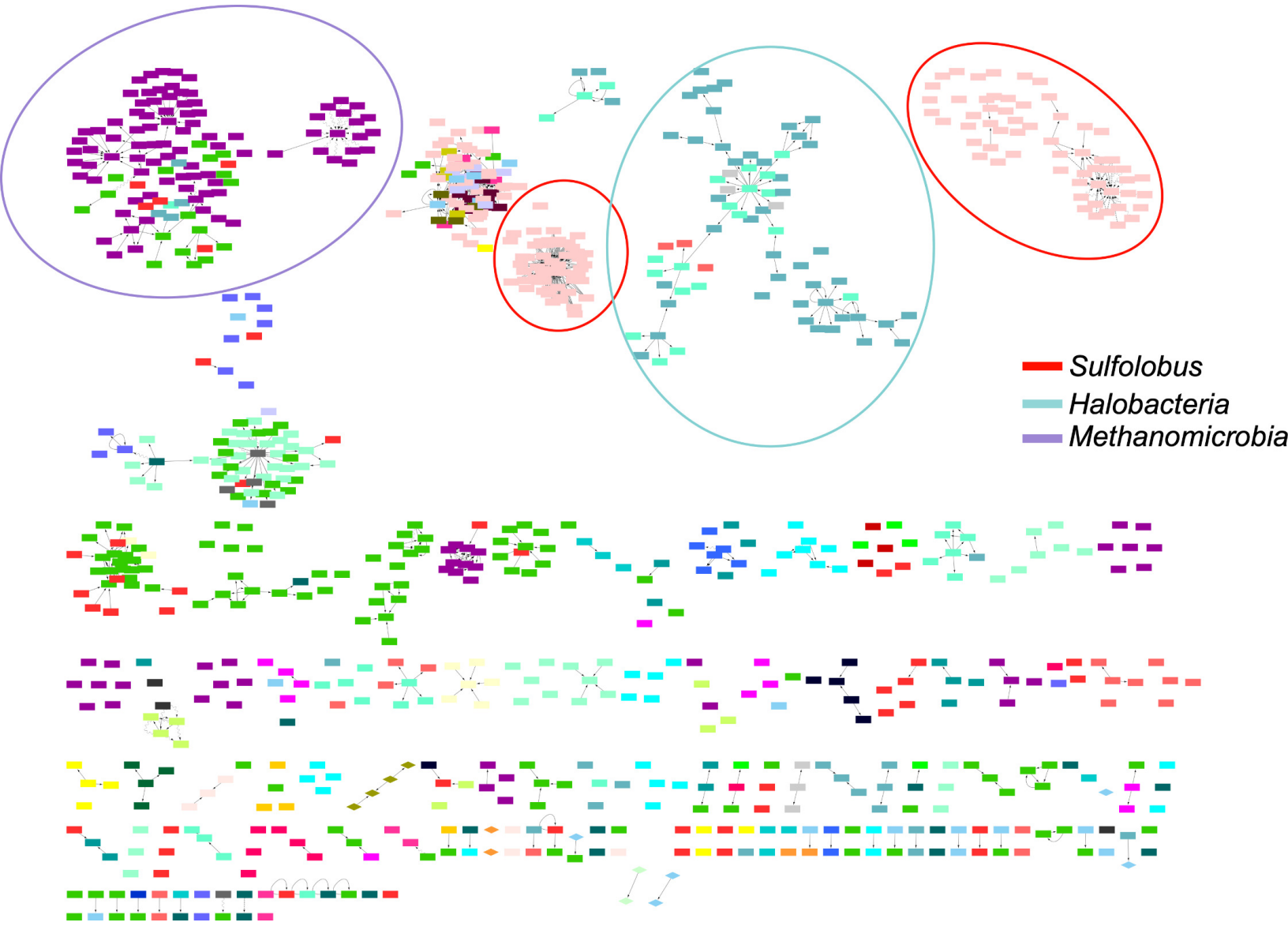
Sulfolobus
Halobacteria
Methanomicrobia